Pan-cancer genomic analysis shows hemizygous *PTEN* loss tumors are associated with immune evasion and poor outcome

Vidotto T [1#], Melo CM [1#], Lautert-Dutra W [1], Chaves LP [1], Reis RB [2], Squire JA[* 1,3]

[#]*Joint first authors*

[1]*Department of Genetics, Medicine School of Ribeirão Preto, University of São Paulo, Ribeirão Preto, Brazil.*

[2] *Division of Urology, Department of Surgery and Anatomy, Medicine School of Ribeirão Preto, University of São Paulo, Ribeirão Preto, Brazil.*

[3] *Department of Pathology and Molecular Medicine, Queen's University, Kingston, Canada.*

** Corresponding author: Jeremy Andrew Squire. E-mail: jsquireinsp@gmail.com*

ABSTRACT

In tumors, somatic mutations of the *PTEN* suppressor gene are associated with advanced disease, chemotherapy resistance, and poor survival. *PTEN* loss of function may occur by inactivating mutation, by deletion, either affecting one copy (hemizygous loss) leading to reduced gene expression or loss of both copies (homozygous) with expression absent. Various murine models have shown that minor reductions in PTEN protein levels strongly influence tumorigenesis. Most *PTEN* biomarker assays dichotomize PTEN (i.e. presence vs. absence) ignoring the role of one copy loss. We performed a *PTEN* copy number analysis of 9,793 TCGA cases from different 30 tumor types. There were 419 (4.28%) homozygous and 2484 (25.37%) hemizygous *PTEN* losses. Hemizygous deletions led to reduced PTEN gene expression, accompanied by increased levels of instability and aneuploidy across tumor genomes. Outcome analysis of the pan-cancer cohort showed that losing one copy of *PTEN* reduced survival and was associated with transcriptomic changes controlling immune response and the tumor microenvironment. Immune cell abundances were significantly altered for *PTEN* loss, with changes in head and neck, cervix, stomach, prostate, brain, and colon more evident in hemizygous loss tumors. These data suggest that reduced expression of *PTEN* in tumors with hemizygous loss leads to tumor progression and influences anticancer immune response pathways.

Keywords PI3K/AKT signaling, haploinsufficiency; tumor suppressor gene; large deletions; somatic mutation; tumor microenvironment; genomic instability; gene dosage; immunotherapy; immune evasion; *in silico* analysis

INTRODUCTION

The PTEN tumor suppressor functions as a phosphatase, which metabolizes PIP3, the lipid product of PI3-Kinase that antagonizes the activation of the oncogenic PI3K/AKT/mTOR signaling axis [1,2]. In addition to its role as a primary regulator of cancer cell growth, recent findings also implicate PTEN in mediating aspects of the immune response against cancer [3,4].

PTEN is frequently lost, either partially affecting one copy of the gene (hemizygous loss; HemDel) or entirely affecting both copies of the gene (homozygous loss; HomDel), in a range of sporadic tumor types. A variety of mechanisms can cause *PTEN* gene inactivation, including missense and truncation mutations and deletions, as well as reduced expression of active PTEN protein mediated by promoter methylation, the effects of miRNAs, and the suppression of PTEN enzyme activity [5]. Loss of function of the *PTEN* tumor suppressor has been observed as one of the most common events in many types of cancer [6], having the greatest selection pressure for deletion based on an analysis of 746 human cancer genomes [7].

The *Pten* conditional knockout mouse model closely mimics human prostate initiation and progression [8]. Studies showed that loss of one copy of the *Pten* allele dramatically increases the rate of tumors [9]. It was proposed that haploinsufficiency of the *Pten* gene resulted in reduced levels of the functional protein that were insufficient for preventing tumor formation. Similar studies using a brain-tumor-specific model also showed that *Pten* haploinsufficiency accelerated the formation of glioblastomas [10]. Analysis of hypomorphic *Pten* mice demonstrated that as little as a 20% reduction of PTEN protein contributed to the development of prostate cancer in mice [11]. These and other mouse studies [12] show that minor reductions in PTEN protein levels can profoundly influence tumorigenesis [13]. The findings from *Pten* murine tumor models are consistent

with the precise cellular controls needed to regulate *PTEN* stability and function [14], implying that even subtle changes in *PTEN* expression may have profound effects on cancer development and progression [5].

Álvarez-Garcia et al. [15] recently surveyed the solid tumor literature on *PTEN* loss resulting from a mutation within the coding region of the gene; hemizygous or homozygous deletions of the gene as assessed by loss of heterozygosity (LOH), reduced copy number in array CGH analysis or loss of *PTEN* by FISH. Most tumor-associated missense mutations resulted in a loss or significantly reduced phosphatase activity or protein truncations. *PTEN* was found to demonstrate distinct patterns of somatic mutation leading to loss of function across different tumor types. Most glioblastomas display loss of function of *PTEN* in agreement with data from TCGA showing *PTEN* deletions in 143/170 (85%) of glioblastomas [16]. Other human tumor types found to have frequent *PTEN* deletions and/or loss of protein are cancers of prostate (25-50%), endometrium (50%), ovary (30-50%), lung (35-55%), breast (30-40%) and colon (10-40%) [17]. Moreover, it was found that single-copy inactivation of *PTEN* was far more common than mutation or deletion of both copies [15]. The PI3K/AKT/mTOR consortium study further suggested that partial copy number *PTEN* loss was associated with a less favorable outcome than complete loss across all available TCGA data [18]. These data, together with the murine *Pten* studies of tumorigenesis, formed the rationale for this PanCancer study that aimed to address the idea that partial loss of function of *PTEN* by hemizygous loss may confer a greater selective advantage for a subset of tumors than complete loss of function by homozygous loss (reviewed in [19]).

Our previous study examining the genomic impact of *PTEN* loss using TCGA data demonstrated that primary prostate tumors harboring *PTEN* deletions had enhanced levels of aneuploidy and non-synonymous mutations [20]. However, it was unclear whether

the genomic instability generated by loss of one copy of *PTEN* was associated with tumor progression. Other studies examining the impact of *PTEN* loss using TCGA and other public domain datasets do not distinguish between one copy loss and complete loss of the gene [21–24]. Similarly, most *PTEN* cancer biomarker studies using immunohistochemistry and fluorescence *in situ* hybridization (FISH) have not been rigorously standardized [15,17,25,26]. For these reasons, the impact of partial loss of function due to one copy loss of *PTEN* is unknown for most cancers.

This study analyzed the TCGA copy-number and transcriptomic data, comparing oncogenic and immunophenotypic features that distinguish hemizygous *PTEN* loss from homozygous loss across the pan-cancer cohort. Our analysis also examines the relationships between *PTEN* intact, hemi-, and homozygous loss with genomic features of tumor progression and disease outcome.

RESULTS

The *PTEN* study group comprised 30 tumors, including 9,793 cases analyzed from the TCGA Pan-cancer cohort. *PTEN* somatic copy number alterations (SCNA) were present in 3,619 (36.96%) tumors. Copy number deletions were observed in 2,903 (29.65%) tumors, with 2,484 (25.37%) having hemizygous deletions resulting in one copy and 419 (4.28%) having homozygous loss of both copies. Copy number gains as a duplication of the *PTEN* gene were evident in 716 (7.31%) tumors (Table 1).

Hemizygous *PTEN* deletions (HemDel) are more common than homozygous deletions (HomDel) across the pan-cancer cohort. For most of the common solid tumors, hemizygous *PTEN* deletions were much more frequent than homozygous deletions (Figure 1). For example, melanoma (SKCM) has 55.86% hemizygous deletion compared to 7.63% homozygous loss. Breast cancer (BRCA) has a hemizygous deletion

frequency of 25.28%, but homozygous deletions are less common at 5.08% of tumors. There are interesting differences in lung subtypes, with squamous cell carcinoma (LUSC) having 44.83% hemizygous and 9.92% homozygous losses. However, adenocarcinoma (LUAD) had fewer hemizygous deletions, 27.50% but only 0.98% homozygous losses. For prostate cancer (PRAD), the rate of hemizygous loss was 14.96%, slightly less than the homozygous loss rate of 17.42%. The four tumor types (KIRP, THYM, THCA, and PCPG) with the lowest frequency of *PTEN* SCNA are characterized by a relatively more favorable outcome in the literature. Pheochromocytoma and paraganglioma (PCPG) are tumors of the autonomic nervous system. This tumor has 6.83% *PTEN* duplication gain suggesting instability leading to *PTEN* acquisition rather than loss may be a feature of this tumor. Other tumors with more marked levels of *PTEN* SCNA gain are ovarian (OV) 19.66%, esophageal carcinoma (ESCA) 12.71%, lung adenocarcinoma (LUAD) 14.34%, stomach adenocarcinoma (STAD) 11.59% and hepatocellular carcinoma of the liver (LIHC) 9.70%.

PTEN expression levels closely correlate to gene copy number. To determine how closely *PTEN* deletions and gains affect *PTEN* expression, we analyzed transcript counts across the pan-cancer cohort to estimate gene expression levels related to *PTEN* copy number (Figure 2a). We observed that tumors with *PTEN* HomDel had the lowest expression levels, with mean transcript counts that were three orders of magnitude lower than the mean count observed in intact tumors. The HemDel tumors showed transcript counts one order of magnitude lower than intact, and *PTEN* gains were associated with slightly higher expression levels than *PTEN* intact tumors. We compared *PTEN* intact to HemDel and HomDel in the cohort's 23 most common solid tumors (Figure 2b). The same reduced expression pattern is apparent in all tumor types, with *PTEN* HomDel having the lowest expression levels for most tumors. Similarly, *PTEN* HemDel exhibited

expression levels that were intermediate between HomDel and *PTEN* intact tumors. These data agree with the general correlations observed between gene copy number and RNA expression levels using TCGA transcriptomic data reported recently [27].

Associations between hemizygous *PTEN* deletions and poor outcome. Analysis of overall survival of the entire cohort stratified by *PTEN* deletion status showed that tumors harboring *PTEN* HemDel had a worse outcome compared with tumors with HomDel and *PTEN* intact (P<0.0001; Figure 3a). We next performed outcome analysis comparing *PTEN* intact to HomDel and HemDel for seven of the common solid tumors (Figure 3b-d and Supplementary Figure a-d). In brain tumors, the *PTEN* intact have a steadily decreased survival probability, but both *PTEN* HomDel and HemDel were associated with a rapid decline in survival probabilities (P<0.0001; Figure 3b). In cervical tumors, there is a lower survival probability for *PTEN* HemDel compared to HomDel and intact (Figure 3c). However, in colorectal tumors, both *PTEN* HemDel and *PTEN* intact showed a worse outcome compared with tumors with *PTEN* HomDel (Figure 3d). In both prostate cancer (Supplementary Figure 1a) and head and neck squamous cell carcinoma (Supplementary Figure 1b), the HemDel tumors were associated with reduced survival probabilities. In stomach tumors (Supplementary Figure 1c), HemDel was associated with intermediate survival risk. Still, in sarcomas (Supplementary Figure 1d), only *PTEN* HomDel presented a worse survival risk, with HemDel carrying a similar survival risk to *PTEN* intact cases.

Relationships between hemizygous *PTEN* deletions and genomic instability. To understand the impact of *PTEN* loss on genomic features of cancer progression, we analyzed the total number of mutations, percent genome altered by losses and gains, intratumor heterogeneity, aneuploidy, and homologous repair defects across the pan-cancer cohort (Figure 4a-d). Our combined analysis revealed that cancers harboring

PTEN HemDel had the highest levels of nonsilent mutations, intratumor heterogeneity, and percent genome altered. Moreover, both *PTEN* HomDel and HemDel presented higher levels of homologous repair defect when compared with *PTEN* intact, but no difference was found between the two deletion types. When stratified by tumor type, many of the tumors harboring *PTEN* deletions had increased levels of nonsilent mutations, intratumor heterogeneity, and homologous repair defects (Supplementary Figure 2a-e). For the comparison of the percentage of genome altered, we found that 65% (13/20) of the investigated tumor types presented elevated genomic alterations when harboring *PTEN* HemDel (Supplementary Figure 2d).

Pan-cancer analysis showed aneuploidy levels were significantly elevated in HemDel compared to HomDel and both deletion types showed significantly increased aneuploidy compared to all intact tumors (Supplementary Figure 3a). Analysis of aneuploidy in a subset of twenty solid tumors showed a general increase in aneuploidy associated with PTEN deletion. Hemizygous losses of bladder, cervix, colon, head and neck, liver, ovarian, pancreatic, and stomach cancer promoted increased levels of aneuploidy (Supplementary Figure 3b). Collectively, these findings led us to hypothesize if *PTEN* HemDel may be associated with an altered transcriptome which could be potentially driving more genomic alterations.

Transcriptomic changes associated with *PTEN* loss activate immune pathways. We next investigated the transcriptome of seven representative solid tumors that had increased frequencies of *PTEN* deletions and presented more diversity in genomic changes. Differential gene expression analyses showed that prostate tumors with *PTEN* HemDel presented 2076 upregulated and 2966 downregulated genes (Supplementary Table 1). Prostate tumors with HemDel of *PTEN* presented several enriched pathways compared with *PTEN* intact, including microtubule-based movement and chromosome

segregation (Supplementary Figure 4). *PTEN* HemDel was also associated with distinct enrichment of immune pathways across the cancer types. In prostate tumors with *PTEN* HomDel the high number of DEGs were linked to cell cycle, DNA repair, and vascular process pathways (Supplementary Figure 5). Interestingly, for HomDel in prostate cancer, the genes closely flanking *PTEN*, such as *ATAD1*, *RNLS* and *KLLN*, are concurrently downregulated with the *PTEN* gene consistent with the large genomic deletions of chromosome 10 previously observed in prostate cancer by FISH [28] (see the vertical bar in Supplementary Figure 5).

Brain tumors presented the most distinct pathway enrichment results, including the upregulation of several immune pathways when *PTEN* was deleted. In these tumors, we found 7841 up- and 6623 downregulated genes when compared tumors with *PTEN* HemDel vs. *PTEN* intact (Supplementary Table 1, Supplementary Figure 6). GO enriched analysis showed that several immune-related pathways were upregulated for *PTEN* HemDel tumors, such as granulocyte migration and chemotaxis, neutrophil migration, acute inflammatory response, humoral immune homeostasis, and many others (Supplementary Figure 6). Similarly, when we compared the transcriptome of tumors with *PTEN* HomDel vs. those with PTEN intact, we observed 6115 up- and 5323 downregulated genes (Supplementary Table 2, Supplementary Figure 7). We also observed that several immune-related pathways were significantly upregulated in brain tumors harboring *PTEN* HomDel, namely myeloid leucocyte migration, humoral immune response, leucocyte chemotaxis, and acute inflammatory response (Supplementary Figure 7). In summary, most investigated tumors had immune-related pathways up- or downregulated when *PTEN* was lost. The RNA-sequencing expression level of immunomodulatory genes like CD274 (PD-L1, Programmed Cell Death), CTLA4 (Cytotoxic T-Lymphocyte Associated Protein 4), IDO1 (Indoleamine 2,3-Dioxygenase

1), and LAG3 (Lymphocyte Activating 3) are altered in breast, glioblastoma, head and neck, liver, ovarian, prostate, sarcoma, stomach, and uterine tumors (Supplementary Figure 8). These findings led us to hypothesize whether *PTEN* genomic deletions may be associated with an altered tumor microenvironment, as determined from higher or lower abundance of immune cells surrounding cancerous lesions.

Stomach tumors harboring *PTEN* HemDel show downregulated immune pathways, such as adaptive immune response, regulation of lymphocyte activation, T cell activation, positive regulation of immune response, leukocyte-mediated immunity, lymphocyte proliferation, and several other pathways (Supplementary Figure 9). Stomach tumors with *PTEN* HemDel also had downregulation of Indoleamine 2,3-Dioxygenase 1 (*IDO1*) gene (Supplementary Figure 9). In contrast, immune pathways were not apparent in stomach tumors harboring *PTEN* HomDel, but the sample size (N=20) for homozygous loss tumors was reduced compared to HemDel tumors (N=90) (Supplementary Figure 10, Supplementary Table 1). For head and neck tumors, we also observed that tumors with *PTEN* HemDel had downregulated immune-related pathways, including adaptive immune response, activation of T-cell receptor, regulation of lymphocyte-mediated immunity, regulation of leukocyte-mediated immunity, and regulation of immune effector process (Figure 5a-c). However, these results were not observed for the comparison between *PTEN* HomDel and *PTEN* intact, in which the sample size from homozygous loss tumors was limited (N=13). However, the linked passenger genes *MINPP1* and *KLLN* from chromosome 10 showed concurrent reduced expression with *PTEN* (Supplementary Figure 11). Lastly, for colon tumors, we found that tumors with *PTEN* HemDel had downregulated immune-related pathways, including response to interferon-gamma, lymphocyte-mediated immunity, adaptive immune response, and natural killer cell-mediated immunity (Supplementary Figure 12). However, effects on

immune pathways were not observed for the comparison between *PTEN* HomDel and *PTEN* intact. As with other homozygous losses, there was reduced expression of a group of *PTEN*-linked passenger genes mapping to chromosome 10, including *ALDH18A1*, *DNMBP*, *KLLN*, *WAPL*, *MINPP1*, and *ATAD1* (see the vertical bar in Supplementary Figure 13). Collectively, the pathway analysis results draw attention to the role hemizygous *PTEN* loss may play in the anticancer immune response.

***PTEN* deletions are associated with an altered tumor immune microenvironment.** The results from the tumor microenvironment comparison of *PTEN* HomDel, HemDel, and intact tumors for all 22 immune cells from brain, prostate, head and neck, and stomach tumors were investigated. *PTEN* HemDel in brain tumors was linked to higher T CD4 memory cells and M2 macrophages abundance and lower M1 macrophages, monocytes, and T CD8 cells (Supplementary Figure 14a). Similar results were seen in head and neck tumors, where *PTEN* HemDel showed higher M0 and M2 macrophages and mast cells and lower CD4+ T-cell, CD8+ T-cell, T-regulatory cells, and NK cells (Figure 5d). While in prostate tumors with *PTEN* HemDel, we observed an increased in M1 macrophages and a decrease in M0 macrophages and monocytes abundance (Supplementary Figure 15b). Stomach tumors with *PTEN* HemDel had an increased plasma and M0 macrophages density and decreased density of CD8+ T-cells (Supplementary Figure 15c). Cervical tumors with *PTEN* HemDel were linked to higher M0 macrophages, and mast cells activated abundance (Supplementary Figure 15d). Similar results were seen in colorectal tumors, where *PTEN* HemDel showed a higher M0 macrophage density and lower CD8+ T-cell abundance (Supplementary Figure 15e).

DISCUSSION

The presence of the PTEN protein is essential for controlling the tumor promoting activities of the PI3K/AKT pathway [2]. Deregulation of this signaling axis confers a strong selective advantage to tumors, so that loss of *PTEN* control by inactivating mutation or deletion is one of the most common somatic events in human cancer [6]. PTEN mutation is significantly related to advanced disease, chemotherapy resistance, and poor survival in patients with head and neck cancers, breast, melanoma, colorectal, esophageal, and prostate [19,29–34] so that its role as a predictive and prognostic cancer biomarker is increasingly gaining prominence [35–37]. Moreover, there is increasing awareness of the role PTEN deficiency plays in shaping the immune landscape in different cancers [3,4].

Various murine models have shown that the tumor-promoting abilities of loss of the *Pten* gene are strongly dose-dependent [38]. In some models, the *Pten* gene loss has been found to exhibit haploinsufficiency with reduced levels of the normal Pten protein resulting in a diversity of tumors in mice [2]. Thus, in contrast to the classical definition of a tumor suppressor gene that requires complete loss of both copies of the gene [39], it appears that reduced amounts of PTEN protein caused by either monoallelic loss or by one inactivating mutation is sufficient to cause cancer (reviewed in [19]).

A recent review across all solid tumors showed that hemizygous *PTEN* loss due to monoallelic deletion or point mutation occurred at a much higher frequency than biallelic loss [15]. Our *PTEN* analysis of TCGA data also shows that most tumors have a much greater frequency of HemDel than HomDel and that hemizygous loss is less favorable than homozygous loss for many tumor types. These data agree with previous genetic and proteomic studies of PI3K/AKT/mTOR axis mutations using TCGA data that showed outcome associated with partial loss of *PTEN* was less favorable than outcome for complete loss of the gene [18]. Our analysis of *PTEN* RNA transcript levels across the

TCGA cohort shows good agreement with gene copy number, as reported recently by others [27], so the HemDel losses we analyzed in this study would be expected to reduce RNA expression levels. Moreover, since one somatic *PTEN* deletion or point mutations leads to a reduction in RNA levels, then partial PTEN protein expression is expected in HemDel tumors.

PTEN deletions and protein loss are known to affect DNA damage responses and disrupt mitotic spindle architecture resulting in accumulation of mutations in other genes and increased chromosome instability in both murine models and human cancers [40]. As expected, our TCGA analysis showed both hemi- and homozygous losses increased genomic instability features in many tumors. However, HemDel tumors had significantly higher rates of non-silent mutations, intratumor heterogeneity, percentage genome altered, and aneuploidy compared to HomDel tumors. This diversity of genetic alteration is likely to facilitate genomic evolution and increase cancer progression, treatment resistance, and poor outcome [41]. Collectively, these data suggest that the elevated levels of genomic instability and somatic mutations in the tumors with hemizygous loss could provide a selective advantage and the less favorable outcome we observe across the TCGA cohort.

The most obvious effects on outcome for HemDel *PTEN* losses were observed in head and neck squamous cell carcinomas (HNSCC) and cervical carcinomas. For both tumor types, hemizygous loss was associated with a less favorable overall survival. *PTEN* loss is associated with poor outcome in HNSCC [30]. HNSCC also has a high frequency of *TP53* somatic mutations [42]. We used cBioPortal to investigate the co-occurrence frequencies of *TP53* mutations with *PTEN* intact, HemDel, and HomDel in HNSCC. Interestingly, *PTEN* HemDel was significantly ($P<0.001$) associated with *TP53* mutation and *PTEN* HomDel was under-represented in HNSCC with mutated *TP53* (data not

shown). These data suggest that there may be preferential selection for one copy of a *PTEN* gene in HNSCC so that reduced levels of the functional PTEN protein allow tumor cells to bypass the *TP53*-induced cell senescence pathway [43]. These observations in HNSCC are in keeping with the *PTEN* literature that suggests that single-copy inactivation of *PTEN* may actually be selected for during the progression of some tumor types since bi-allelic inactivation of *PTEN* has been shown to lead to senescence or cell death when *TP53* is mutated [5]. Recent functional studies of the relationship between *TP53* mutation and *PTEN* loss in HNSCC indicate that loss of regulation of both pathways could influence radio- and chemosensitivity [44]. These findings are also in agreement with recent studies showing that *PTEN* loss mediates resistance to cetuximab in HNSCC, indicating the need for more treatment response *PTEN* predictive biomarker studies in this tumor that also examined the role of HemDel events [45].

Mouse models of HNSCC draw attention to the role of *Pten* in the evasion of cellular senescence and activation of cancer-related inflammation [46]. Our gene set enrichment analysis for HNSCC indicates that various pathways involved with immune activation are downregulated in *PTEN* HemDel tumors. Pathways indicated in our analysis were antigen presentation, interferon, interleukins, toll-like, neutrophil, B cell, and inflammasome signaling. More marked alterations to the immune response in HemDel HNSCC were also evident in our CIBERSORT analysis. There were decreased CD8+ve T-cells and alterations to TAMs consistent with the immune tumor microenvironment being less favorable in hemizygous HNSCC. These findings are consistent with the emerging recognition that *PTEN* loss could be a useful predictive immune biomarker in HNSCC [47].

Biomarker analysis of colorectal cancer showed weak expression of the PTEN protein in primary tumors was associated with acquisition metastatic disease [33]. Our study

found that *PTEN* HemDel colorectal tumors had downregulated immune-related pathways. Functional activities associated with immune response included regulation of granulocyte-macrophage colony-stimulating factor production, neutrophil migration, and regulation of leukocyte-mediated cytotoxicity. These findings are consistent with recent studies that showed that PTEN mutation was associated with microsatellite stability/instability and tumor mutational burden in colon cancer [48]. Both *in vitro* studies [49] and recent analyses of colon tumors [50] suggest that *PTEN* loss in colorectal carcinoma may activation of PI3K and upregulate *PD-L1* expression. These data are in keeping with other studies indicating that the PTEN/ PI3K axis may promote immune escape through regulating *PDL1/PD1* expression [3,51].

Brain tumors also presented distinct pathway enrichment findings, including the upregulation of several immune pathways for *PTEN* HemDel and HomDel losses. These data are consistent with a recent study showing *PTEN* loss in glioblastoma was associated with immunosuppressive expression signatures and failed response to anti-PD-1 immunotherapy [52].

Our TCGA analysis of prostate tumors with *PTEN* HemDel identified elevated levels of genomic instability and an increase in M1 macrophages but decreased abundances of M0 macrophages and monocytes. Pathway analysis showed enrichment for response to type I-interferon, consistent with other recent findings showing that *PTEN* loss leads to an immunosuppressive microenvironment in PCa [53]. These conclusions also agree with our previous study that showed increased IDO1 and Tregs in the prostate cancer tumor microenvironment [54]. Interestingly, analysis of PCa showed that the genes flanking *PTEN*, such as *ATAD1*, *RNLS*, and *KLLN* are concurrently down-regulated when the *PTEN* gene is homozygously deleted. Similar observations were made in both colon and head and neck tumors with homozygous deletions. These data suggest that large

somatic deletions of chromosome 10 may often encompass closely linked genes whose expression changes could contribute to clinical phenotypes [36].

Unfortunately, most previous *PTEN* cancer biomarker studies have not systematically analyzed mutations or deletions using molecular genetic methods that can distinguish between HemDel and HomDel mutations. Similarly, loss of the protein using immunohistochemistry as an alternative way of determining PTEN status has also not been studied using uniform, reproducible methods that can detect subtle changes in protein levels [15,17,25,26]. The end result has been that majority of published *PTEN* cancer biomarker studies have depended on a variety of simple two-way classification assays (*PTEN* loss vs. intact) that ignore the distinction between hemi- and homozygous losses.

Our study also has some limitations that need to be addressed in future *PTEN* analyses of the highlighted tumors. Our work was based entirely on *in silico* analysis of copy number data derived TCGA, and all the pathway and immune parameters were inferred from the associated transcriptome data. The analysis presented here cannot fully capture the impact of PTEN mutations based on the limitations of the TCGA dataset, which lacks prognostic or treatment information. Also, our expression analyses associated with *PTEN* status were, like all *in silico* TCGA studies, obtained from the bulk tumors containing heterogeneous tumor cells intermingled with a small subset of stromal cells and varying quantities of immune cells. Lastly, our analysis regarding *PTEN* status did not include *PTEN* inversions, fusions, promoter methylations, and large-scale structural variants, which may be a source of bias in our evaluation of the impact of HemDel and HomDel effects.

Collectively, our findings based on TCGA, together with the extensive murine *Pten* studies by others [8,9], suggest that loss of one copy of *PTEN* by mutation or deletion may be sufficient to promote tumorigenesis and anti-cancer immune evasion. However,

for most human cancers, there have been limited biomarker studies on how hemizygous *PTEN* deletion and partial protein loss may influences outcome and treatment response.

METHODS

Data download and processing

We initially downloaded raw and level 3 PanCancer normalized RNAseq, array-CGH, and SNV from 10,713 samples derived from 31 tumor types from The Cancer Genome Atlas (TCGA) cohort (www.gdc.cancer.gov). These initial cases were used to determine outcome, genomic alterations, and relative immune abundances. For the differential gene expression analysis (DEG), TCGA biolinks had 9793 cases were available from 30 primary tumors as detailed in Table 1.

Raw RNAseq experiments were performed through Illumina HiSeq 2000 RNA Sequencing platform. Copy number data were obtained from array-CGH experiments performed with the Affymetrix Genome-Wide Human SNP Array 6.0. DNA sequencing was performed in Illumina Genome Analyzer DNA sequencing. Clinical data for progression-free intervals and overall survival were obtained for all patients from the TCGA cohort. All analyses were conducted with data derived from primary tumors.

Defining *PTEN* deletions

PTEN deletions were characterized by using GISTIC-derived categorical somatic copy number alterations (SCNA). In brief, GISTIC identifies a cutoff for copy number loss or gain using the log2 continuous data from each individual segments, such as genes and other regions [55]. These analyses were performed by the TCGA group for the PanCancer analysis. We obtained, for our study, the Level 3 copy number calls for *PTEN* gene resulting from whole genome detection of copy number changes or point mutations inactivating either one or both copies of the gene [20]. The calls were defined as HomDel

(two copies with loss/mutation), HemDel (one copy loss or mutation), intact *PTEN* (both copies present without mutation), and duplications of the *PTEN* gene [56]. *PTEN* duplications consisted of the presence of gain of an extra copy of the entire gene or regions at 10q23.31 that included *PTEN*.

Gene expression and enrichment analyses.

Analysis of gene expression was performed on the RNAseq level. Raw read counts for TCGA-tumors were downloaded using FANTOM-CAT/recount2 (https://jhubiostatistics.shinyapps.io/recount/) [57,58]. The subset of samples was compiled using each patient's clinical information, and only primary tumors were used in the analysis. Study groups were divided based on *PTEN* status, HomDel (two copies with loss/mutation), HemDel (one copy loss or mutation), and Intact *PTEN* (both copies present without mutation). Differential expression (DE) analysis was carried out using DESeq2 (v 1.32.0) [59,60]. For enrichment analysis of DE genes, we used the clusterProfile package (v 3.18.1) [61,62]. We used a P-adjusted value < 0.05 as the cutoff for the enrichment results. All analyses were conducted in RStudio software (R Foundation for Statistical Computing, R v4.1.2) and all results were plotted by ggplot2 [63].

***In silico* analysis of immune abundance in tumor types**

To estimate the immune cell landscape in each tumor, we used the CIBERSORT deconvolution method (https://cibersort.stanford.edu/) which is an established tool to determine the abundance of immune cells using whole-transcriptome data [64]. We separately imputed normalized gene expression data of brain, prostate, head and neck, stomach, cervical and colorectal tumors from the TCGA cohort.

REFERENCES

1. Liu, T., Wang, Y., Wang, Y. & Chan, A. M. Multifaceted regulation of PTEN subcellular distributions and biological functions. *Cancers (Basel).* **11**, (2019).
2. Chalhoub, N. & Baker, S. J. PTEN and the PI3-kinase pathway in cancer. *Annu. Rev. Pathol.* **4**, 127–150 (2009).
3. Vidotto, T. *et al.* Emerging role of PTEN loss in evasion of the immune response to tumours. *Br. J. Cancer* **122**, 1732–1743 (2020).
4. Bezzi, M. *et al.* Diverse genetic-driven immune landscapes dictate tumor progression through distinct mechanisms. *Nat. Med.* **24**, 165–175 (2018).
5. Lee, Y., Chen, M. & Pandolfi, P. P. The functions and regulation of the PTEN tumour suppressor: new modes and prospects. *Nat. Rev. Mol. Cell Biol.* **19**, 547–562 (2018).
6. The ICGC/TCGA Pan-Cancer Analysis of Whole Genomes Consortium. Pan-cancer analysis of whole genomes. *Nature* **578**, 82–93 (2020).
7. Bignell, G. R. *et al.* Signatures of mutation and selection in the cancer genome. *Nature* **463**, 893–898 (2010).
8. Wang, S. *et al.* Prostate-specific deletion of the murine Pten tumor suppressor gene leads to metastatic prostate cancer. *Cancer Cell* **4**, 209–221 (2003).
9. Kwabi-Addo, B. *et al.* Haploinsufficiency of the Pten tumor suppressor gene promotes prostate cancer progression. *Proc. Natl. Acad. Sci. U. S. A.* **98**, 11563–11568 (2001).
10. Kwon, C. H. *et al.* Pten haploinsufficiency accelerates formation of high-grade astrocytomas. *Cancer Res.* **68**, 3286–3294 (2008).
11. Alimonti, A. *et al.* Subtle variations in Pten dose determine cancer susceptibility. *Nat. Genet.* **42**, 454–458 (2010).

12. Shen-Li, H., Koujak, S., Szablocs, M. & Parsons, R. Reduction of Pten dose leads to neoplastic development in multiple organs of PtenshRNA mice. *Cancer Biol. Ther.* **10**, 1194–1200 (2010).

13. Carracedo, A., Alimonti, A. & Pandolfi, P. P. PTEN level in tumor suppression: How much is too little? *Cancer Res.* **71**, 629–633 (2011).

14. Masson, G. R. & Williams, R. L. Structural mechanisms of PTEN regulation. *Cold Spring Harb. Perspect. Med.* **10**, (2020).

15. Álvarez-Garcia, V., Tawil, Y., Wise, H. M. & Leslie, N. R. Mechanisms of PTEN loss in cancer: It's all about diversity. *Semin. Cancer Biol.* **59**, 66–79 (2019).

16. Brennan, C. W. *et al.* The somatic genomic landscape of glioblastoma. *Cell* **155**, 462–77 (2013).

17. Pulido, R. *et al.* Precise immunodetection of PTEN protein in human neoplasia. *Cold Spring Harb. Perspect. Med.* **9**, 1–30 (2019).

18. Zhang, Y. *et al.* A Pan-Cancer Proteogenomic Atlas of PI3K/AKT/mTOR Pathway Alterations. *Cancer Cell* **31**, 820-832.e3 (2017).

19. Berger, M. F. *et al.* The genomic complexity of primary human prostate cancer. *Nature* **470**, 214–220 (2011).

20. Vidotto, T., Tiezzi, D. G. & Squire, J. A. Distinct subtypes of genomic PTEN deletion size influence the landscape of aneuploidy and outcome in prostate cancer. *Mol. Cytogenet.* **11**, 1 (2018).

21. Fan, C., Zhao, C., Shugen Li, F. W. & Wang, J. Significance of PTEN mutation in cellular process, prognosis, and drug selection in clear cell renal cell carcinoma. *Front. Oncol.* **9**, 1–9 (2019).

22. Sun, J., Li, S., Wang, F., Fan, C. & Wang, J. Identification of key pathways and genes in pten mutation prostate cancer by bioinformatics analysis. *BMC Med.*

Genet. **20**, 1–9 (2019).

23. Imada, E. L. *et al.* Transcriptional landscape of PTEN loss in primary prostate cancer. *BMC Cancer* **21**, 1–13 (2021).

24. Lin, Z. *et al.* PTEN loss correlates with T cell exclusion across human cancers. *BMC Cancer* **21**, 1–14 (2021).

25. Jamaspishvili, T. *et al.* Clinical implications of PTEN loss in prostate cancer. *Nat. Rev. Urol.* **15**, 222–234 (2018).

26. Hocking, C. *et al.* Can we accurately report PTEN status in advanced colorectal cancer? *BMC Cancer* **14**, 1–7 (2014).

27. Shao, X. *et al.* Copy number variation is highly correlated with differential gene expression: A pan-cancer study. *BMC Med. Genet.* **20**, 1–14 (2019).

28. Yoshimoto, M. *et al.* PTEN genomic deletions that characterize aggressive prostate cancer originate close to segmental duplications. *Genes, Chromosom. Cancer* **51**, 149–160 (2012).

29. da Costa, A. A. B. A. *et al.* Low PTEN expression is associated with worse overall survival in head and neck squamous cell carcinoma patients treated with chemotherapy and cetuximab. *Int. J. Clin. Oncol.* **20**, 282–289 (2015).

30. Nagata, Y. *et al.* PTEN activation contributes to tumor inhibition by trastuzumab, and loss of PTEN predicts trastuzumab resistance in patients. *Cancer Cell* **6**, 117–127 (2004).

31. Bucheit, A. D. *et al.* Complete loss of PTEN protein expression correlates with shorter time to brain metastasis and survival in stage IIIB/C melanoma patients with BRAFV600 mutations. *Clin. Cancer Res.* **20**, 5527–5536 (2014).

32. Tachibana, M. *et al.* Expression and Prognostic Significance of PTEN Product Protein in Patients with Esophageal Squamous Cell Carcinoma. *Cancer* **94**, 1955–

1960 (2002).

33. Sawai, H. *et al.* Loss of PTEN expression is associated with colorectal cancer liver metastasis and poor patient survival. *BMC Gastroenterol.* **8**, 1–7 (2008).

34. Sircar, K. *et al.* PTEN genomic deletion is associated with p-Akt and AR signalling in poorer outcome, hormone refractory prostate cancer. *J. Pathol.* **218**, 505–513 (2009).

35. Bazzichetto, C. *et al.* Pten as a prognostic/predictive biomarker in cancer: An unfulfilled promise? *Cancers (Basel).* **11**, 1–22 (2019).

36. Poluri, R. T. K. & Audet-Walsh, É. Genomic deletion at 10q23 in prostate cancer: More than PTEN loss? *Front. Oncol.* **8**, 1–7 (2018).

37. Fusco, N. *et al.* Pten alterations and their role in cancer management: Are we making headway on precision medicine? *Genes (Basel).* **11**, 1–19 (2020).

38. Carnero, A. & Paramio, J. M. The PTEN/PI3K/AKT Pathway in vivo, cancer mouse models. *Front. Oncol.* **4**, 1–10 (2014).

39. Wang, L. H., Wu, C. F., Rajasekaran, N. & Shin, Y. K. Loss of tumor suppressor gene function in human cancer: An overview. *Cell. Physiol. Biochem.* **51**, 2647–2693 (2018).

40. Hou, S. Q., Ouyang, M., Brandmaier, A., Hao, H. & Shen, W. H. PTEN in the maintenance of genome integrity: From DNA replication to chromosome segregation. *BioEssays* **39**, 1–9 (2017).

41. Salk, J. J., Fox, E. J. & Loeb, L. A. Mutational Heterogeneity in Human Cancers: Origin and Consequences. *Annu. Rev. Pathol. Mech. Dis.* **5**, 51–75 (2010).

42. Lawrence, M. S. *et al.* Comprehensive genomic characterization of head and neck squamous cell carcinomas. *Nature* **517**, 576–582 (2015).

43. Chen, Z. *et al.* Crucial role of p53-dependent cellular senescence in suppression of

Pten-deficient tumorigenesis. *Nature* **436**, 725–730 (2005).

44. Vahabi, M. *et al.* MiR-96-5p targets PTEN expression affecting radio-chemosensitivity of HNSCC cells. *J. Exp. Clin. Cancer Res.* **38**, 1–16 (2019).

45. Izumi, H. *et al.* Pathway-specific genome editing of PI3K/mTOR tumor suppressor genes reveals that PTEN loss contributes to cetuximab resistance in head and neck cancer. *Mol. Cancer Ther.* **19**, 1562–1571 (2020).

46. Bian, Y. *et al.* Loss of TGF-β signaling and PTEN promotes head and neck squamous cell carcinoma through cellular senescence evasion and cancer-related inflammation. *Oncogene* **31**, 3322–3332 (2012).

47. dos Santos, L. V., Abrahão, C. M. & William, W. N. Overcoming Resistance to Immune Checkpoint Inhibitors in Head and Neck Squamous Cell Carcinomas. *Front. Oncol.* **11**, 1–16 (2021).

48. Serebriiskii, I. G. *et al.* Comprehensive characterization of PTEN mutational profile in a series of 34,129 colorectal cancers. *Nat. Commun.* **13**, (2022).

49. Song, M. *et al.* PTEN Loss Increases PD-L1 Protein Expression and Affects the Correlation between PD-L1 Expression and Clinical Parameters in Colorectal Cancer. *PLoS One* **8**, (2013).

50. Ugai, T. *et al.* Association of PIK3CA mutation and PTEN loss with expression of CD274 (PD-L1) in colorectal carcinoma . *Oncoimmunology* **10**, 1956173 (2021).

51. Lastwika, K. J. *et al.* Control of PD-L1 expression by oncogenic activation of the AKT-mTOR pathway in non-small cell lung cancer. *Cancer Res.* **76**, 227–238 (2015).

52. Zhao, J. *et al.* Immune and genomic correlates of response to anti-PD-1 immunotherapy in glioblastoma. *Nat. Med.* **25**, 462–469 (2019).

53. Imada, E. L. *et al.* Transcriptional landscape of PTEN loss in primary prostate cancer. *bioRxiv* 1–42 (2020).

54. Vidotto, T. . *et al.* PTEN-deficient prostate cancer is associated with an immunosuppressive tumor microenvironment mediated by increased expression of IDO1 and infiltrating FoxP3+ T regulatory cells. *Prostate* **1**, 1–11 (2019).

55. Mermel, C. H. *et al.* GISTIC2.0 facilitates sensitive and confident localization of the targets of focal somatic copy-number alteration in human cancers. *Genome Biol.* **12**, 1–14 (2011).

56. Zack, T. I. *et al.* Pan-cancer patterns of somatic copy number alteration. *Nat. Genet.* **45**, 1134–1140 (2013).

57. Collado-Torres, L. *et al.* Reproducible RNA-seq analysis using recount2. *Nat. Biotechnol.* **35**, 319–321 (2017).

58. Imada, E. L. *et al.* Recounting the FANTOM CAGE-Associated Transcriptome. *Genome Res.* **30**, 1073–1081 (2020).

59. Love, M. I., Huber, W. & Anders, S. Moderated estimation of fold change and dispersion for RNA-seq data with DESeq2. *Genome Biol.* **15**, 1–21 (2014).

60. Zhu, A., Ibrahim, J. G. & Love, M. I. Heavy-Tailed prior distributions for sequence count data: Removing the noise and preserving large differences. *Bioinformatics* **35**, 2084–2092 (2019).

61. Liberzon, A. *et al.* The Molecular Signatures Database Hallmark Gene Set Collection. *Cell Syst.* **1**, 417–425 (2015).

62. Wu, T. *et al.* clusterProfiler 4.0: A universal enrichment tool for interpreting omics data. *Innov.* **2**, 100141 (2021).

63. Wickham, H. *ggplot2: Elegant Graphics for Data Analysis. Springer-Verlag New York. Media* vol. 35 (2016).

64. Newman, A. M. *et al.* Robust enumeration of cell subsets from tissue expression profiles. *Nat. Methods* 1–10 (2015).

DECLARATIONS

Authors' contributions: All authors contributed equally to the development of this study. All authors read and approved the final manuscript.

Competing interests: The authors declare that they have no competing interests

Availability of data and materials: All data used in this analysis can be found at the GDC data portal. The code and processed data were provided as supplementary materials.

Ethics approval and consent to participate: Research Ethics Committee of the Clinical Hospital of the Faculty of Medicine of Ribeirão Preto, number 3.088.034.

Funding: This research was funded by FAPESP, grant numbers 2019/22912-8 (JAS), 2021/12271-5 (WLD), and 2020/12816-9 (LPC) and by CNPq grant PQ-1D to JAS.

Figures

Figure 1. Relative percentages of *PTEN* Somatic Copy Number Alterations (*PTEN* SCNA) from the 23 most common solid tumors taken from the 30 tumor types analyzed in the Pan-cancer cohort (shown in Table 1). Hemizygous deletions (HemDel) = blue; Homozygous deletions (HomDel) = red, Intact (no *PTEN* SCNA) = green, and gain/duplication = brown. The tumors are ranked by their combined frequencies of PTEN deletion (HemDel + HomDel) with melanomas (SKCM) having the highest overall frequency of *PTEN* deletion (top) and Pheochromocytoma and Paraganglioma (PCPG) having the lowest (bottom). Duplication or *PTEN* gain (Dupl) was not included in the rank order determination.

Figure 2. (**a**) Combined analysis of the association between *PTEN* SCNA status and differential gene expression of PTEN for all 30 tumors in the Pan-cancer cohort. Boxplots show the relationship between PTEN normalized transcript counts Log^2 (Y-axis) versus *PTEN* SCNA status (HemDel, HomDel, Dupl and Intact). The mean transcript count for *PTEN* intact was 18.69, HomDel was the lowest expression level at 17.06 and HemDel showed reduced expression at 18.22 but Dupl was slightly higher than intact at 18.84. The mean transcript counts for all three classes of SCNA significantly deviated $P<0.05$ from intact. (**b**) Association between *PTEN* SCNA status and differential gene expression of PTEN for the 23 most common solid tumors in the Pan-cancer cohort. Boxplots show the relationship between PTEN transcript counts Log^2 (Y-axis) versus *PTEN* SCNA

status HomDel (red), HemDel (blue), and Intact (green) for each tumor. For the majority of tumors the mean transcript counts for both HomDel and HemDel deviated significantly P<0.05 from intact.

Figure 3. Kaplan-Meier curves illustrate overall survival for both *PTEN* intact and *PTEN* deletions groups (HemDel and HomDel). Boxplots (**a**) Pan-cancer cohort shows a lower survival probability for *PTEN* HemDel compared to HomDel and intact (P<0.0001). (**b**) Brain tumors (GBM + LGG) show that both HomDel and HemDel are equally associated with earlier events (P<0.0001). (**c**) Cervical tumors show a lower survival probability for *PTEN* HemDel compared to HomDel and intact. (**d**) Colorectal tumors show a lower survival probability for *PTEN* HemDel compared to HomDel.

Figure 4. *PTEN* deletions are associated with (**a**) increased mutation levels, (**b**) intra tumor heterogeneity (ITH), (**c**) homologous repair defects (HRD), and (**d**) percent genome alteration. Hemizygous deletions of *PTEN* are associated with increased levels of genomic alterations compared with homozygous deletions. Intact *PTEN* showed the lowest levels of genomic alterations.

Figure 5. *PTEN* HemDel in head and neck squamous cell carcinoma (HNSC) shows distinct transcriptome activity. (**a**) Transcriptome heatmap exhibiting clustering of top 50 DEGs. The color scale in the heatmap represents the Z-score of the normalized read counts for each gene, where the red scale color indicates upregulated, and blue low expressed genes. Enrichment analyses were performed using *clusterProfiler* and *p*-adjusted value = 0.05 as the cutoff. (**b**) Enriched GO (BP) pathways of the upregulated genes. (**c**) Enriched GO (BP) pathways of the downregulated genes. The tables shown in (b) and (c) indicate the top 10 most significant Gene Ontology (BP) terms. *: *p*-value < 0.05; **: *p*-value < 0.01, by Mann-Whitney test. n=492 (**d**) CIBERSORT-derived immune-cell abundance of 22 distinct cell subsets based on *PTEN* status and head and neck tumors. Y-axis shows CIBERSORT relative scores. *PTEN* HemDel in head and neck tumors was linked to higher M0 and M2 macrophages and mast cells and lower T CD4, T CD8, T regs, and NK cells. DC, dendritic cell; NK, natural-killer cell; PCa, prostate cancer; Treg, regulatory T cell; M0, M0 macrophage; M1, M1 macrophage; M2, M2 macrophage.

Table 1. *PTEN* somatic copy number status (SCNA). HemDel: *PTEN* hemizygous deletion. HomDel: *PTEN* homozygous deletion. *Dupl* Duplication or gain across the Pan-cancer cohort of 30 tumors. ACC - Adrenocortical carcinoma, BLCA - Bladder Urothelial Carcinoma, BRCA - Breast invasive carcinoma, Brain (LGG - Brain Lower Grade Glioma combined with glioblastoma GBM), CESC - Cervical squamous cell carcinoma and endocervical adenocarcinoma, COAD - Colon adenocarcinoma, DLBC - Lymphoid Neoplasm Diffuse Large B - cell Lymphoma, ESCA - Esophageal carcinoma, HNSC - Head and Neck squamous cell carcinoma, KICH – kidney chromophobe, KIRC - Kidney renal clear cell carcinoma, KIRP - Kidney renal papillary cell carcinoma, LIHC - Liver hepatocellular carcinoma, LUAD - Lung adenocarcinoma, LUSC – Lung Squamous Squamous Cell Carcinoma, MESO - Mesothelioma, OV - Ovarian serous cystadenocarcinoma, PAAD - Pancreatic adenocarcinoma, PCPG - Pheochromocytoma and Paraganglioma, PRAD, Prostate Adenocarcinoma, READ - Rectum adenocarcinoma,

SARC - Sarcoma, SKCM - Skin Cutaneous Melanoma, STAD - Stomach adenocarcinoma, TGCT - Testicular Germ Cell Tumors, THCA - Thyroid carcinoma, THYM - Thymoma, UCEC - Uterine Corpus Endometrial Carcinoma, UCS - Uterine Corpus Endometrial Carcinoma, UVM - Uveal Melanoma.

Supplementary figures

Supplementary Figure 1. Kaplan-Meier survival analysis comparing *PTEN* intact with both *PTEN* deletions groups (HemDel and HomDel). (**a**) Prostate cancer. (**b**) Head and neck cancer. (**c**) Stomach tumors. (**d**) Sarcoma.

Supplementary Figure 2. *PTEN* deletions are associated with genomic alterations in each tumor type. (**a**) Nonsilent mutations. (**b**) Intratumor heterogeneity. (**c**) Homologous repair defects. (**d**) Percent genome altered.

Supplementary Figure 3. Association between aneuploidy levels and *PTEN* inactivation status. (**a**) *PTEN* inactivation is significantly associated with increased levels of aneuploidy. (**b**) Aneuploidy score stratified by tumor type. Prostate and brain tumors showed the lowest levels of aneuploidy across tumor types. Aneuploidy levels were determined based on the length of copy number alterations and normalized by tumor type. The scores range from 0, which indicates low levels of chromosome aberrations (copy number gains and losses). On the other hand, high levels of aneuploidy indicate that the genome of these tumors is highly altered, with larger chromosome gains and losses occurring.

Supplementary Figure 4. *PTEN* HemDel PRAD showed distinct transcriptome activity. (**a**) Transcriptome heatmap exhibiting clustering of top 50 DEGs. (**b**) Enriched GO (BP) pathways of the upregulated genes. (**c**) Enriched GO (BP) pathways of the downregulated genes. The color scale in the heatmap represents the Z-score of the normalized read counts for each gene, where the red scale color indicates upregulated and blue low expressed genes. Enrichment analyses were performed using *clusterProfiler* and *p*-adjusted value = 0.05 as the cutoff. Tables show the top 10 most significant Gene Ontology (BP) terms.

Supplementary Figure 5. *PTEN* HomDel PRAD showed distinct transcriptome activity. **a)** Transcriptome heatmap exhibiting clustering of top 50 DEGs. **b)** Enriched GO (BP) pathways of the upregulated genes. **c)** Enriched GO (BP) pathways of the downregulated genes. The color scale in the heatmap represents the Z-score of the normalized read counts for each gene, where the red scale color indicates upregulated and blue low expressed genes. Enrichment analyses were performed using *clusterProfiler* and *p*-adjusted value = 0.05 as the cutoff. Tables show the top 10 most significant Gene Ontology (BP) terms. Vertical bar indicates the closely linked passenger genes (*ATAD1, RNLS* and *KLLN*) that are concurrently down-regulated when *PTEN* is lost by a large deletion of chromosome 10.

Supplementary Figure 6. *PTEN* HemDel Brain (GBM + LGG) showed distinct transcriptome activity. (**a**) Transcriptome heatmap exhibiting clustering of top 50 DEGs. (**b**) Enriched GO (BP) pathways of the upregulated genes. (**c**) Enriched GO (BP) pathways of the downregulated genes. The color scale in the heatmap represents the Z-

score of the normalized read counts for each gene, where the red scale color indicates upregulated and blue low expressed genes. Enrichment analyses were performed using *clusterProfiler* and *p*-adjusted value = 0.05 as the cutoff. Tables show the top 10 most significant Gene Ontology (BP) terms.

Supplementary Figure 7. *PTEN* HomDel Brain (GBM + LGG) showed distinct transcriptome activity. (**a**) Transcriptome heatmap exhibiting clustering of top 50 DEGs. (**b**) Enriched GO (BP) pathways of the upregulated genes. The color scale in the heatmap represents the Z-score of the normalized read counts for each gene, where the red scale color indicates upregulated and blue low expressed genes. Enrichment analyses were performed using *clusterProfiler* and *p*-adjusted value = 0.05 as the cutoff. Tables show the top 10 most significant Gene Ontology (BP) terms.

Supplementary Figure 8. The RNA-sequencing expression level of immunomodulatory genes *CD274* (*PD-L1*), *CTLA4*, *IDO1*, and *LAG3* in BRCA, GBM, HNSC, LIHC, OV, PRAD, SARC, STAD, and UCS. *: *p*-value < 0.05; **: *p*-value < 0.01, by Mann-Whitney test. *CD274* (*PD-L1*), Programmed Cell Death 1 Ligand 1; *CTLA4*, Cytotoxic T-Lymphocyte Associated Protein 4; *IDO1*, Indoleamine 2,3-Dioxygenase 1; LAG3, Lymphocyte Activating 3.

Supplementary Figure 9. *PTEN* HemDel STAD showed distinct transcriptome activity. (**a**) Transcriptome heatmap exhibiting clustering of top 50 DEGs. (**b**) Enriched GO (BP) pathways of the upregulated genes. (**c**) Enriched GO (BP) pathways of the downregulated genes. The color scale in the heatmap represents the Z-score of the normalized read counts for each gene, where the red scale color indicates upregulated and blue low expressed genes. Enrichment analyses were performed using *clusterProfiler* and *p*-adjusted value = 0.05 as the cutoff. Tables show the top 10 most significant Gene Ontology (BP) terms.

Supplementary Figure 10. *PTEN* HomDel STAD showed distinct transcriptome activity. (**a**) Transcriptome heatmap exhibiting clustering of top 50 DEGs. (**b**) Enriched GO (BP) pathways of the upregulated genes. The color scale in the heatmap represents the Z-score of the normalized read counts for each gene, where the red scale color indicates upregulated and blue low expressed genes. Enrichment analyses were performed using *clusterProfiler* and *p*-adjusted value = 0.05 as the cutoff. Tables show the top 10 most significant Gene Ontology (BP) terms.

Supplementary Figure 11. *PTEN* HomDel HNSC showed distinct transcriptome activity. (**a**) Transcriptome heatmap exhibiting clustering of top 50 DEGs. (**b**) Enriched GO (BP) pathways of the upregulated genes. (**c**) Enriched GO (BP) pathways of the downregulated genes. The color scale in the heatmap represents the Z-score of the normalized read counts for each gene, where the red scale color indicates upregulated and blue low expressed genes. Enrichment analyses were performed using *clusterProfiler* and *p*-adjusted value = 0.05 as the cutoff. Tables show the top 10 most significant Gene Ontology (BP) terms. Vertical bar indicates the two closely linked passenger genes (*MINPP1 and KLLN*) that are concurrently down-regulated when PTEN is lost by a large deletion of chromosome 10.

Supplementary Figure 12. *PTEN* HemDel COAD showed distinct transcriptome activity. (**a**) Transcriptome heatmap exhibiting clustering of top 50 DEGs. (**b**) Enriched

GO (BP) pathways of the downregulated genes. The color scale in the heatmap represents the Z-score of the normalized read counts for each gene, where the red scale color indicates upregulated and blue low expressed genes. Enrichment analyses were performed using *clusterProfiler* and *p*-adjusted value = 0.05 as the cutoff. Tables show the top 10 most significant Gene Ontology (BP) terms.

Supplementary Figure 13. *PTEN* HomDel COAD showed distinct transcriptome activity. Transcriptome heatmap exhibiting clustering of top 50 DEGs. Vertical bar indicates the closely linked passenger genes (*ALDH18A1*, *DNMBP*, *KLLN*, *WAPL*, *MINPP1*, *ATAD1)* that are concurrently down-regulated when PTEN is lost by a large deletion of chromosome 10.

Supplementary Figure 14. CIBERSORT-derived immune-cell abundance of 22 distinct cell subsets based on *PTEN* status and tumor type. Y-axis shows CIBERSORT relative scores. (**a**) *PTEN* HemDel in brain tumors was linked to higher T CD4 memory cells and M2 macrophage abundance and lower M1 macrophages, monocytes, and T CD8 cells. (**b**) Prostate tumors with *PTEN* HemDel showed increased M1 macrophages and decreased M0 macrophages and monocytes. (**c**) Stomach tumors with *PTEN* HemDel showed increased plasma and M0 macrophages and decreased in T CD8 cells. (**d**) Cervical tumors with *PTEN* HemDel were linked to higher M0 macrophages and mast cells activated. (**e**) Colorectal tumors with *PTEN* HemDel were linked to higher M0 macrophages and lower T CD8 cells. DC, dendritic cell; NK, natural-killer cell; PCa, prostate cancer; Treg, regulatory T cell; M0, M0 macrophage; M1, M1 macrophage; M2, M2 macrophage. *: *p*-value < 0.05; **: *p*-value < 0.01, by Mann-Whitney test.

Supplementary Table 1. The number of differentially expressed genes (DE Genes) comparing HemDel and HomDel to intact in seven solid tumors. FDR < 0.05. *PTEN* deletion status: HemDel: *PTEN* hemizygous deletion. HomDel: *PTEN* homozygous deletion. Int: *PTEN* intact.

Figure 1

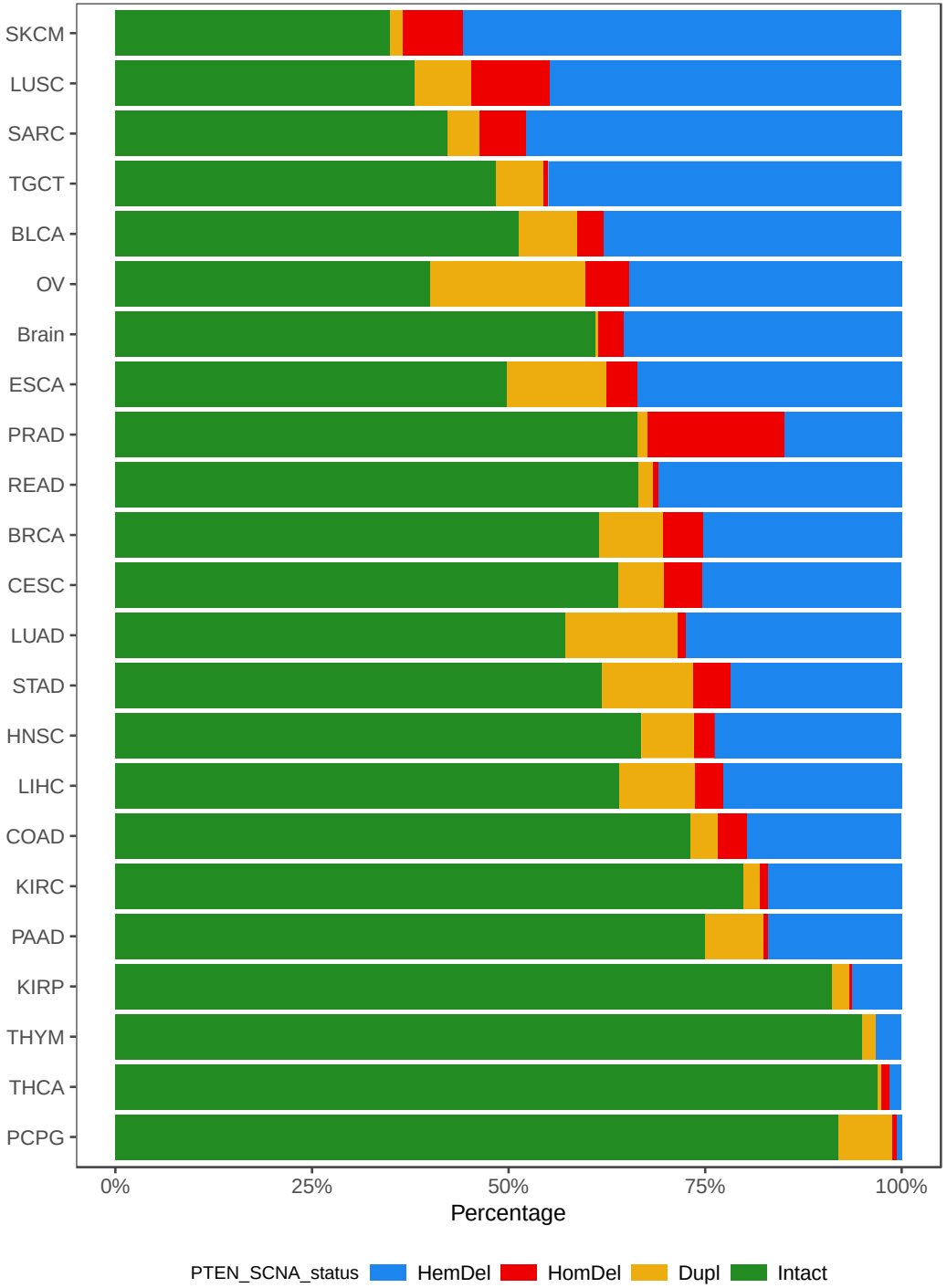
SKCM
LUSC
SARC
TGCT
BLCA
OV
Brain
ESCA
PRAD
READ
BRCA
CESC
LUAD
STAD
HNSC
LIHC
COAD
KIRC
PAAD
KIRP
THYM
THCA
PCPG
0%
25%
50%
75%
100%
Percentage
PTEN_SCNA_status
HemDel
HomDel
Dupl
Intact

Figure 2

a

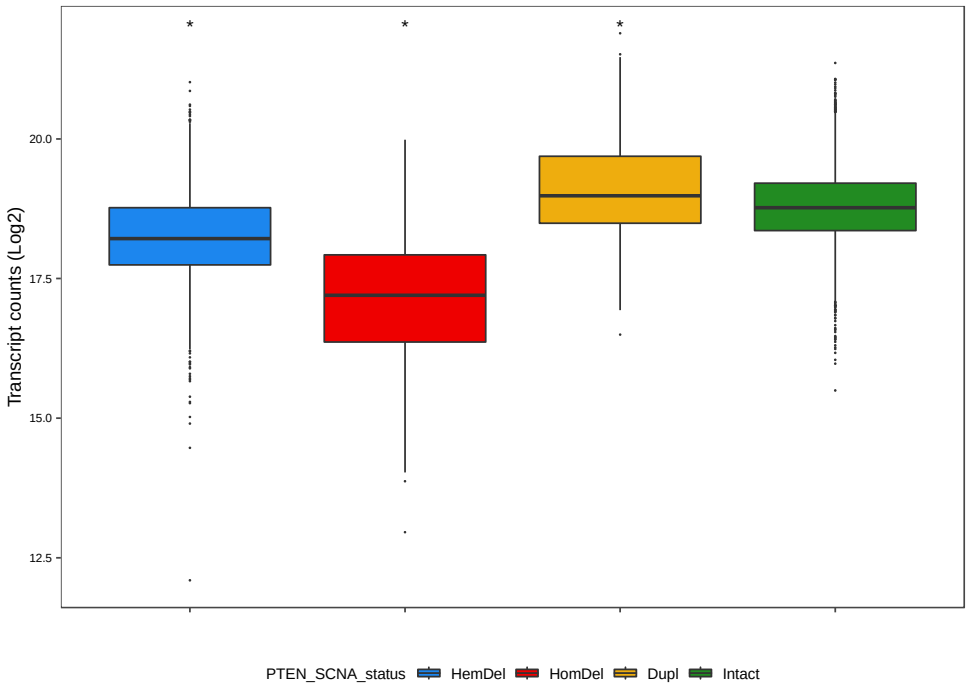
Transcript counts (Log2)
20.0
17.5
15.0
12.5
PTEN_SCNA_status
HemDel
HomDel
Dupl
Intact

b

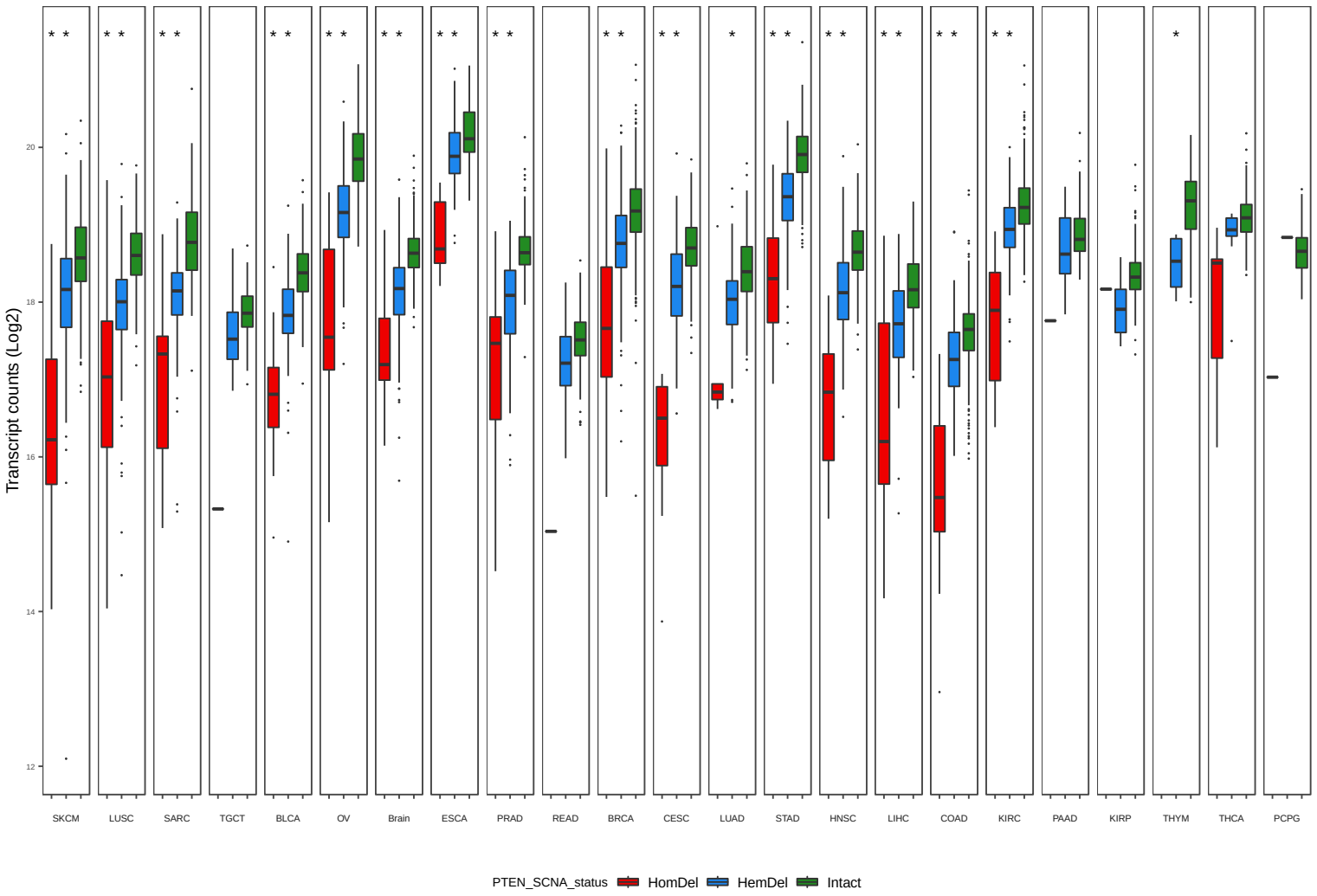
Transcript counts (Log2)
20
18
16
14
12
SKCM
LUSC
SARC
TGCT
BLCA
OV
Brain
ESCA
PRAD
READ
BRCA
CESC
LUAD
STAD
HNSC
LIHC
COAD
KIRC
PAAD
KIRP
THYM
THCA
PCPG
PTEN_SCNA_status
HomDel
HemDel
Intact

Figure 3

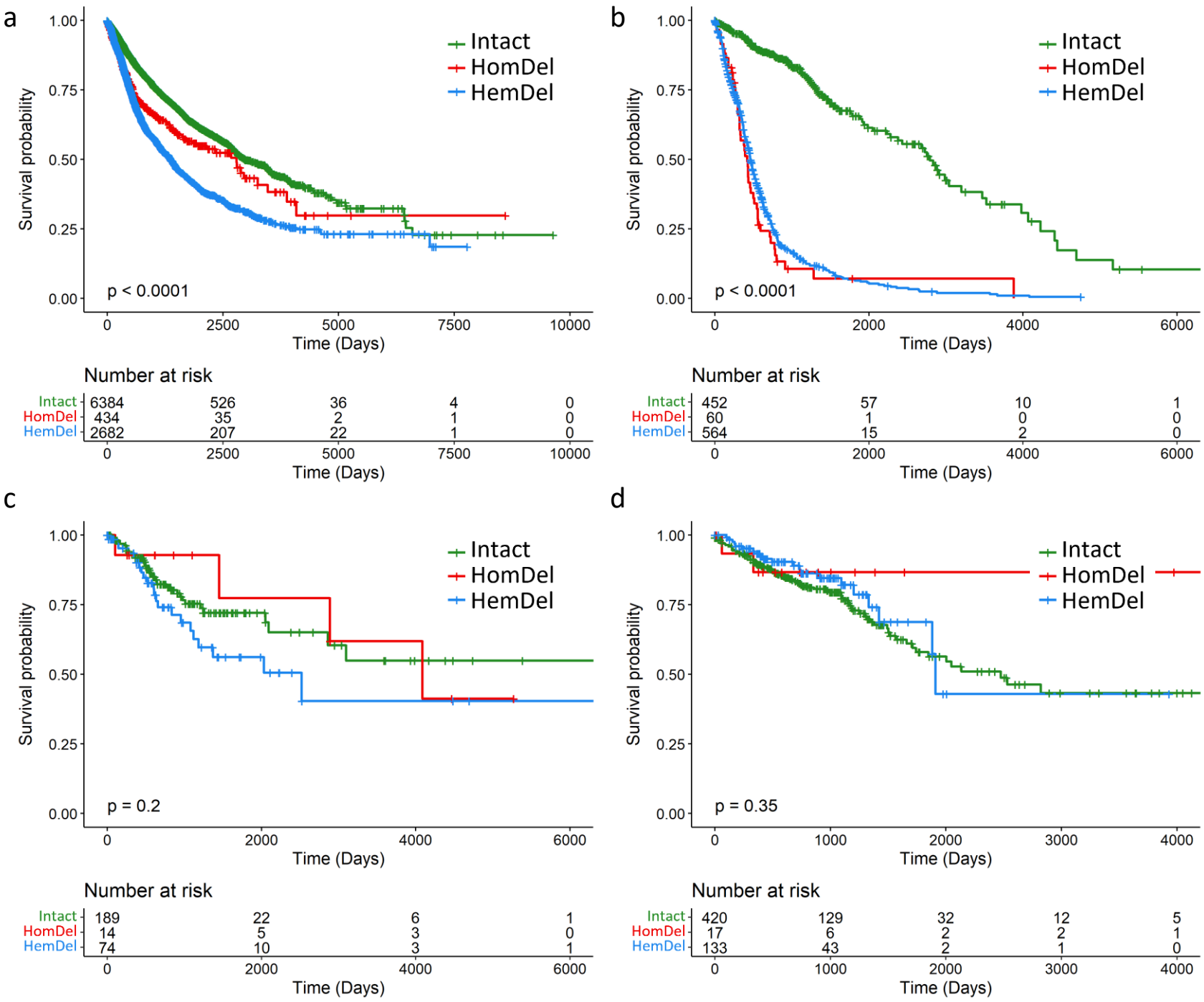
a
Survival probability
1.00
0.75
0.50
0.25
0.00
Intact
HomDel
HemDel
p < 0.0001
0
2500
5000
7500
10000
Time (Days)
Number at risk
Intact 6384 526 36 4 0
HomDel 434 35 2 1 0
HemDel 2682 207 22 1 0
b
Survival probability
p < 0.0001
0
2000
4000
6000
Time (Days)
Number at risk
Intact 452 57 10 1
HomDel 60 1 0 0
HemDel 564 15 2 0
c
Survival probability
p = 0.2
Time (Days)
Number at risk
Intact 189 22 6 1
HomDel 14 5 3 0
HemDel 74 10 3 1
d
Survival probability
p = 0.35
0
1000
2000
3000
4000
Time (Days)
Number at risk
Intact 420 129 32 12 5
HomDel 17 6 2 2 1
HemDel 133 43 2 1 0

Figure 4

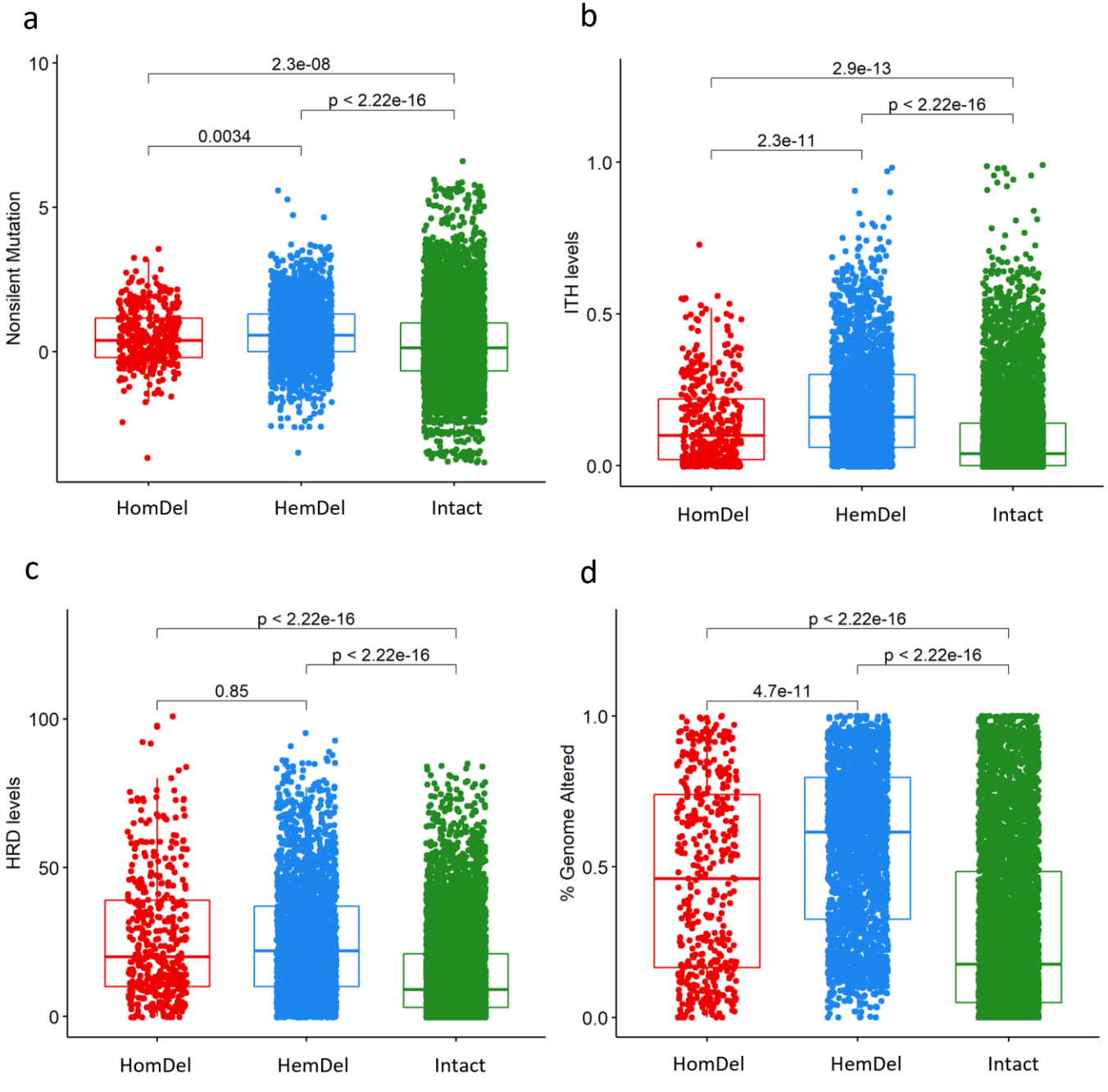
a
Nonsilent Mutation
10
5
0
2.3e-08
p < 2.22e-16
0.0034
HomDel
HemDel
Intact
b
ITH levels
1.0
0.5
0.0
2.9e-13
p < 2.22e-16
2.3e-11
HomDel
HemDel
Intact
c
HRD levels
100
50
0
p < 2.22e-16
p < 2.22e-16
0.85
HomDel
HemDel
Intact
d
% Genome Altered
1.0
0.5
0.0
p < 2.22e-16
p < 2.22e-16
4.7e-11
HomDel
HemDel
Intact

Figure 5

a

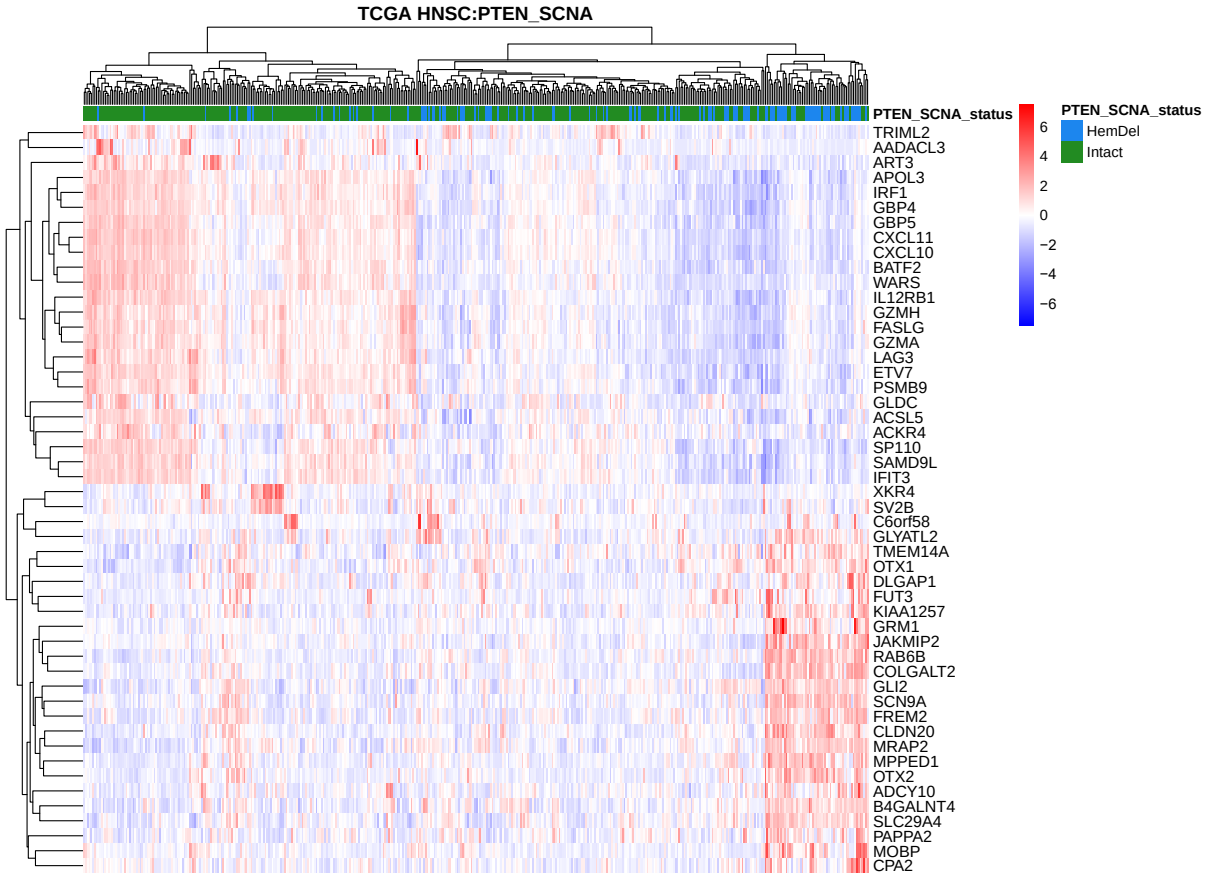

b

ID	Description	qvalue
GO:0002250	adaptive immune response	2,90E-53
GO:0002449	lymphocyte mediated immunity	1,34E-27
GO:0050778	positive regulation of immune response	2,30E-27
GO:0042110	T cell activation	2,75E-27
GO:0051249	regulation of lymphocyte activation	4,96E-22
GO:0002697	regulation of immune effector process	9,23E-20
GO:0007159	leukocyte cell-cell adhesion	3,95E-17
GO:0032943	mononuclear cell proliferation	9,05E-17
GO:0001819	positive regulation of cytokine production	1,26E-15
GO:0046651	lymphocyte proliferation	1,38E-15

c

ID	Description	qvalue
GO:0050804	modulation of chemical synaptic transmission	0.0012
GO:0099177	regulation of trans-synaptic signaling	0.0012
GO:0009953	dorsal/ventral pattern formation	0.0012
GO:0006749	glutathione metabolic process	0.0029
GO:0007409	axonogenesis	0.0097
GO:0071466	cellular response to xenobiotic stimulus	0.0116
GO:0030900	forebrain development	0.0183
GO:0007224	smoothened signaling pathway	0.0183
GO:0060571	morphogenesis of an epithelial fold	0.0183
GO:0060572	morphogenesis of an epithelial bud	0.0183

d

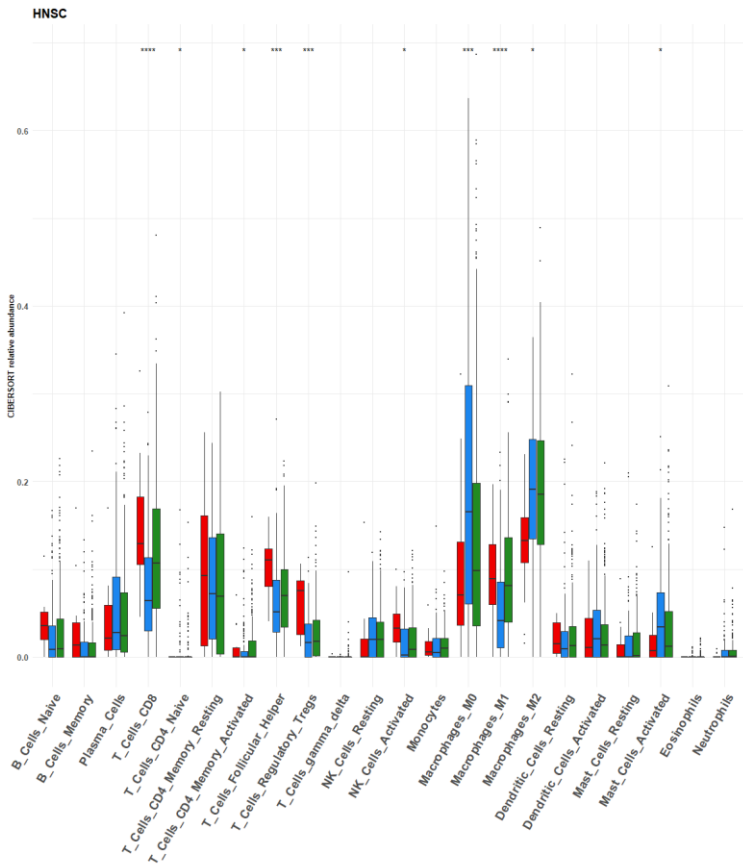

Table 1

	PTEN CNA Status								
TCGA Study	HemDel	%	HomDel	%	Dupl	%	Intact	%	Total
ACC	8	10,39	1	1,30	22	28,57	46	59,74	77
BLCA	153	37,87	14	3,47	30	7,43	207	51,24	404
BRCA	269	25,28	54	5,08	87	8,18	654	61,47	1064
Brain	235	35,34	22	3,31	2	0,30	406	61,05	665
CESC	74	25,43	14	4,81	17	5,84	186	63,92	291
COAD	86	19,72	16	3,67	15	3,44	319	73,17	436
DLBC	4	8,33	3	6,25	5	10,42	36	75,00	48
ESCA	61	33,70	7	3,87	23	12,71	90	49,72	181
HNSC	117	23,78	13	2,64	33	6,71	329	66,87	492
KICH	47	72,31	1	1,54	2	3,08	15	23,08	65
KIRC	86	17,03	5	0,99	11	2,18	403	79,80	505
KIRP	18	6,36	1	0,35	6	2,12	258	91,17	283
LIHC	82	22,71	13	3,60	35	9,70	231	63,99	361
LUAD	140	27,50	5	0,98	73	14,34	291	57,17	509
LUSC	217	44,83	48	9,92	35	7,23	184	38,02	484
MESO	25	28,74	2	2,30	3	3,45	57	65,52	87
OV	143	34,71	23	5,58	81	19,66	165	40,05	412
PAAD	30	17,05	1	0,57	13	7,39	132	75,00	176
PCPG	1	0,62	1	0,62	11	6,83	148	91,93	161
PRAD	73	14,96	85	17,42	6	1,23	324	66,39	488
READ	48	30,97	1	0,65	3	1,94	103	66,45	155
SARC	120	47,81	15	5,98	10	3,98	106	42,23	251
SKCM	205	55,86	28	7,63	6	1,63	128	34,88	367
STAD	90	21,74	20	4,83	48	11,59	256	61,84	414
TGCT	67	44,97	1	0,67	9	6,04	72	48,32	149
THCA	8	1,62	5	1,01	2	0,40	480	96,97	495
THYM	4	3,36	0	0,00	2	1,68	113	94,96	119
UCEC	53	10,23	19	3,67	108	20,85	338	65,25	518
UCS	19	33,93	1	1,79	18	32,14	18	32,14	56
UVM	1	1,25	0	0,00	0	0,00	79	98,75	80
	2484	25,37	419	4,28	716	7,31	6174	63,05	9793

Supplementary figures and tables

Supplementary table 1

				DE Genes (HemDel vs Intact)		DE Genes (HomDel vs Intact)	
Tumor type	HemDel	HomDel	Int	Up	Down	Up	Down
Brain	235	22	406	7841	6623	6115	5323
Colorectal	86	16	319	1086	1536	23	175
Cervix	74	14	186	728	649	743	512
Head and Neck	117	13	329	1727	1842	444	1148
Prostate	73	85	324	2076	2966	3304	3835
Sarcoma	120	15	106	2032	3725	241	708
Stomach	90	20	256	3216	2814	683	1434
	795	185	1926	18706	20155	11553	13135

Supplementary figure 1

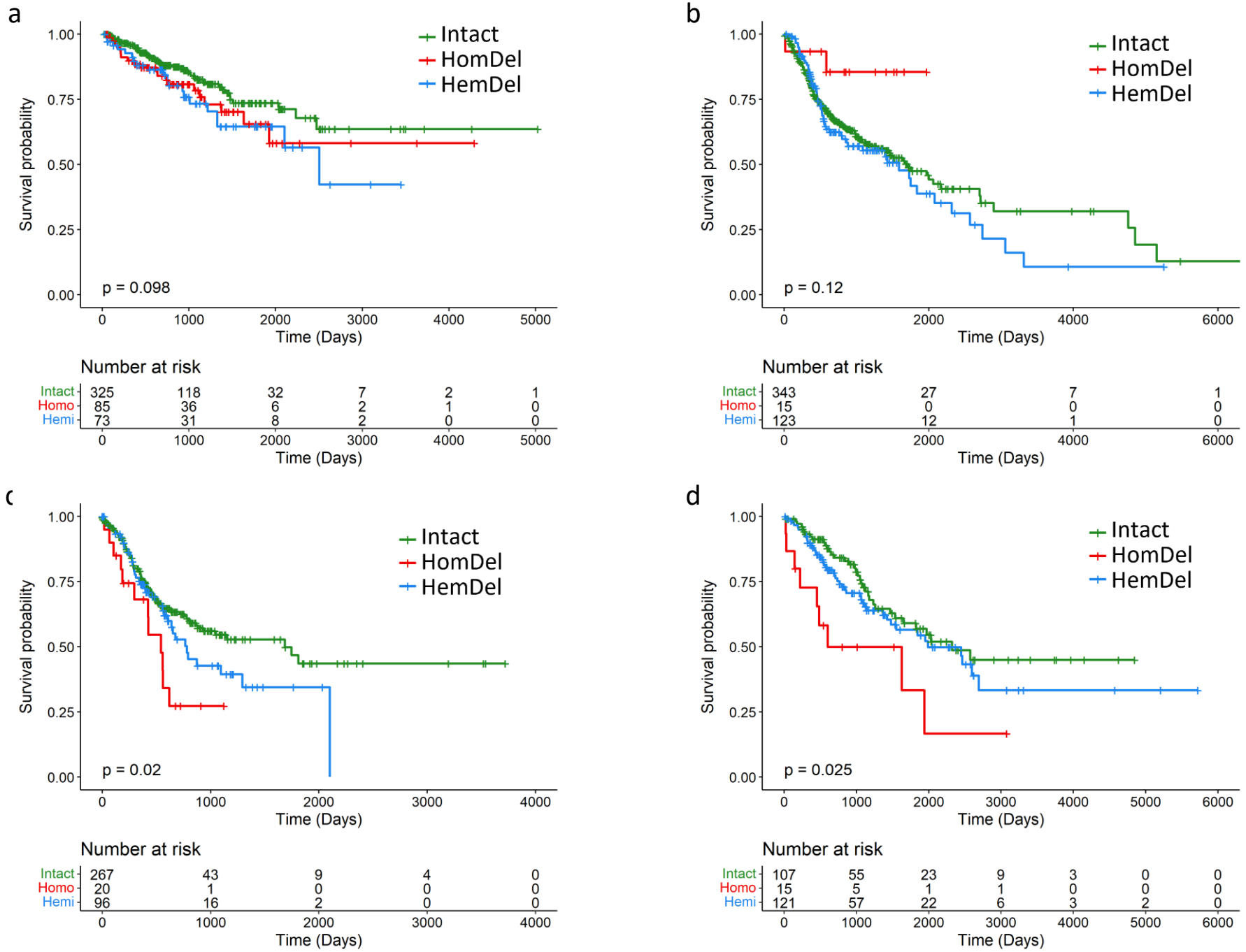

Supplementary figure 2

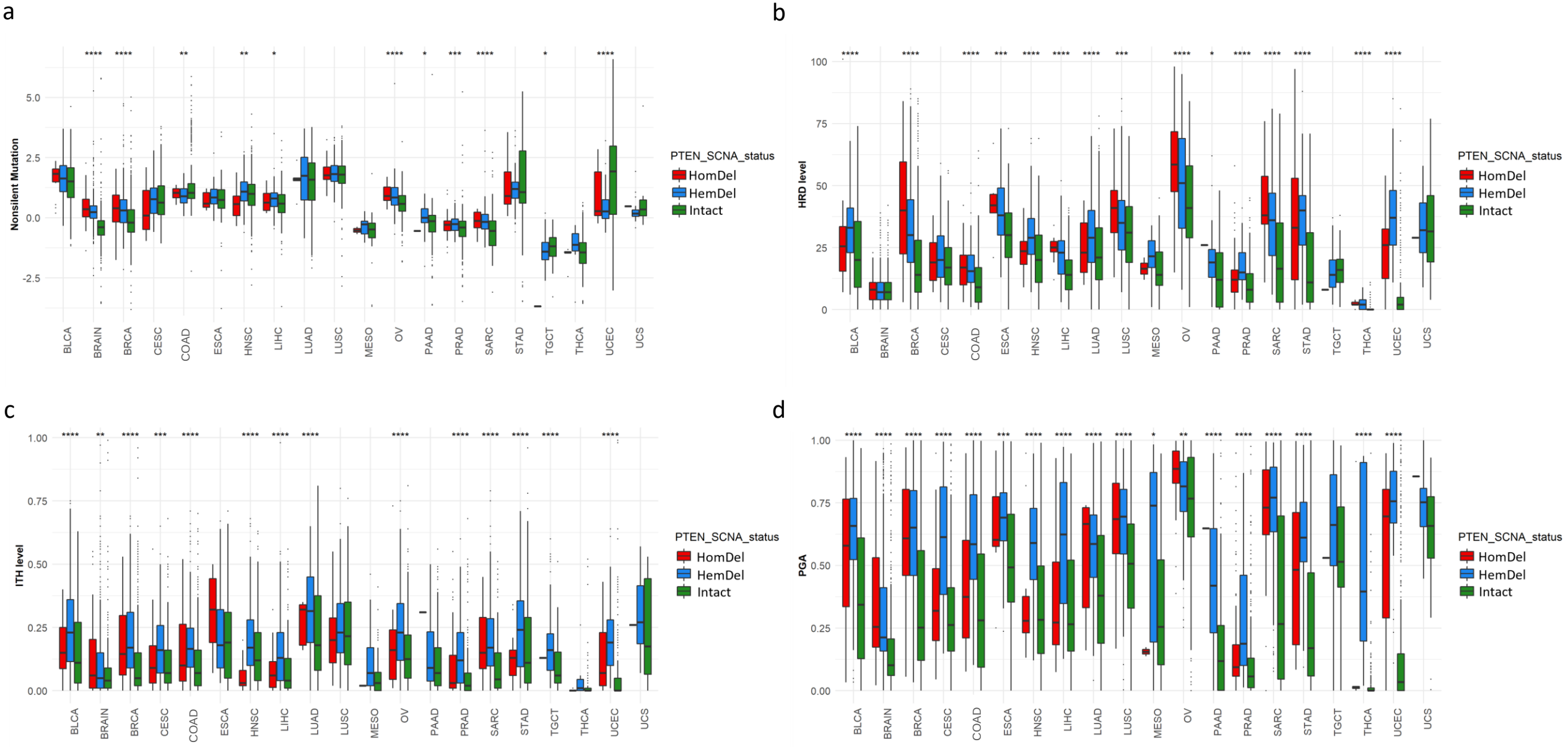

Supplementary figure 3

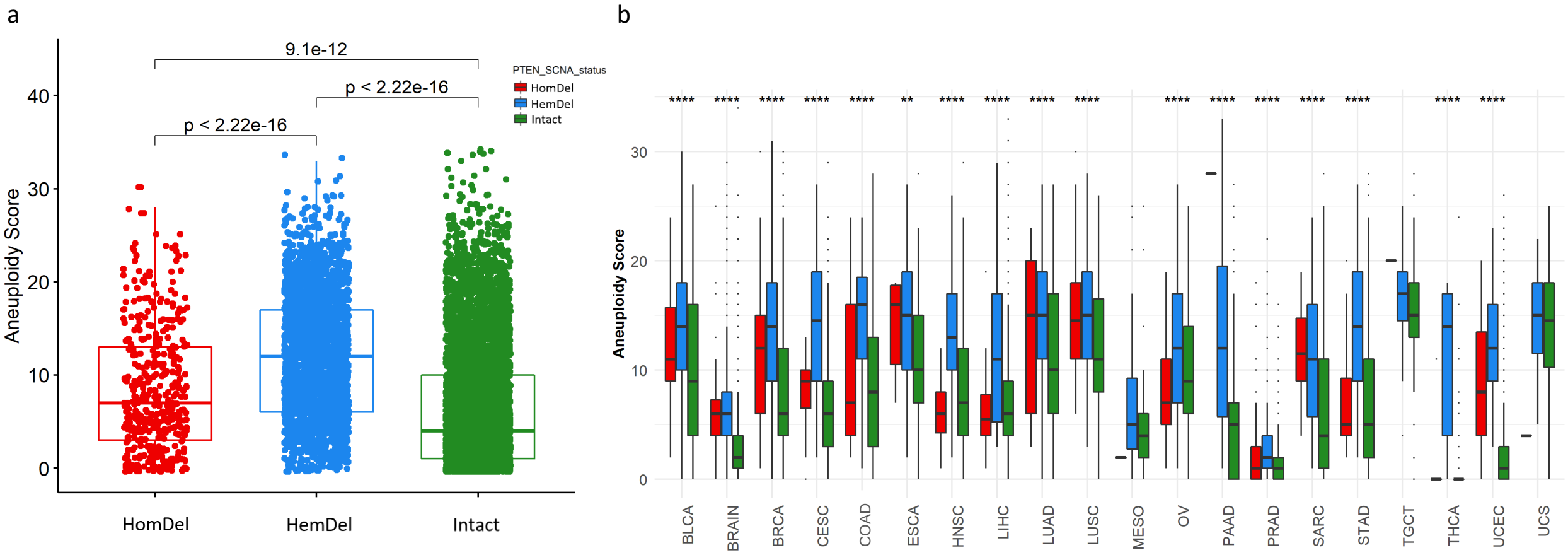

Supplementary figure 4

a

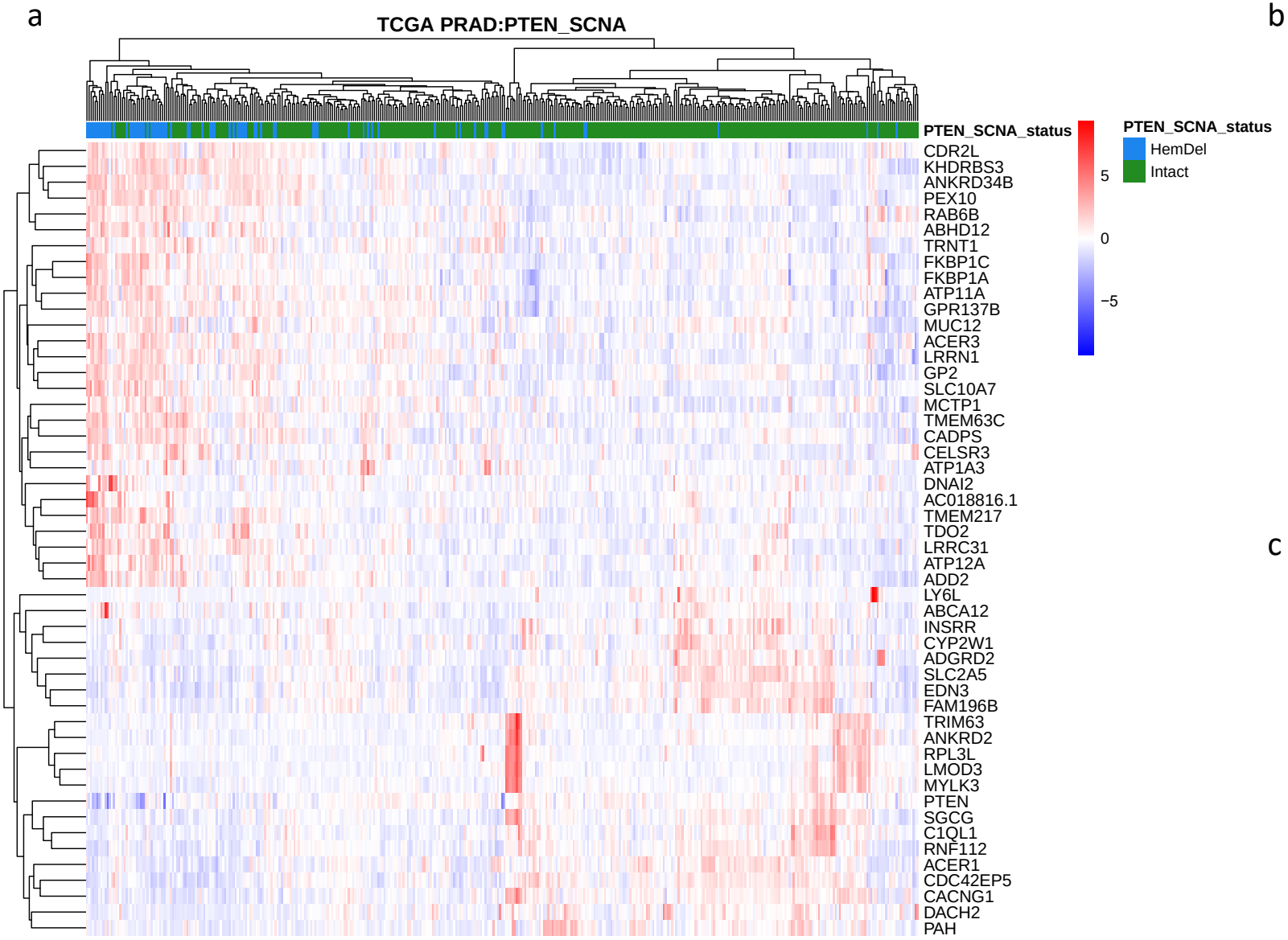

b

ID	Description	qvalue
GO:0007018	microtubule-based movement	3,41E+11
GO:0007059	chromosome segregation	3,41E+11
GO:0000070	mitotic sister chromatid segregation	3,41E+11
GO:0098813	nuclear chromosome segregation	0.0011
GO:1902850	microtubule cytoskeleton organization involved in mitosis	0.0015
GO:0034329	cell junction assembly	0.0018
GO:0050808	synapse organization	0.0028
GO:0032886	regulation of microtubule-based process	0.0038
GO:0000280	nuclear division	0.0065
GO:0007156	homophilic cell adhesion via plasma membrane adhesion molecules	0.0072

c

ID	Description	qvalue
GO:0002181	cytoplasmic translation	3,03E+07
GO:0006936	muscle contraction	1,28E+10
GO:0016054	organic acid catabolic process	1,86E+11
GO:0044282	small molecule catabolic process	8,90E+11
GO:0008015	blood circulation	0.0020
GO:0086005	ventricular cardiac muscle cell action potential	0.0070
GO:0010273	detoxification of copper ion	0.0154
GO:1990169	stress response to copper ion	0.0154
GO:0061687	detoxification of inorganic compound	0.0174
GO:0086009	membrane repolarization	0.0174

Supplementary figure 5

a

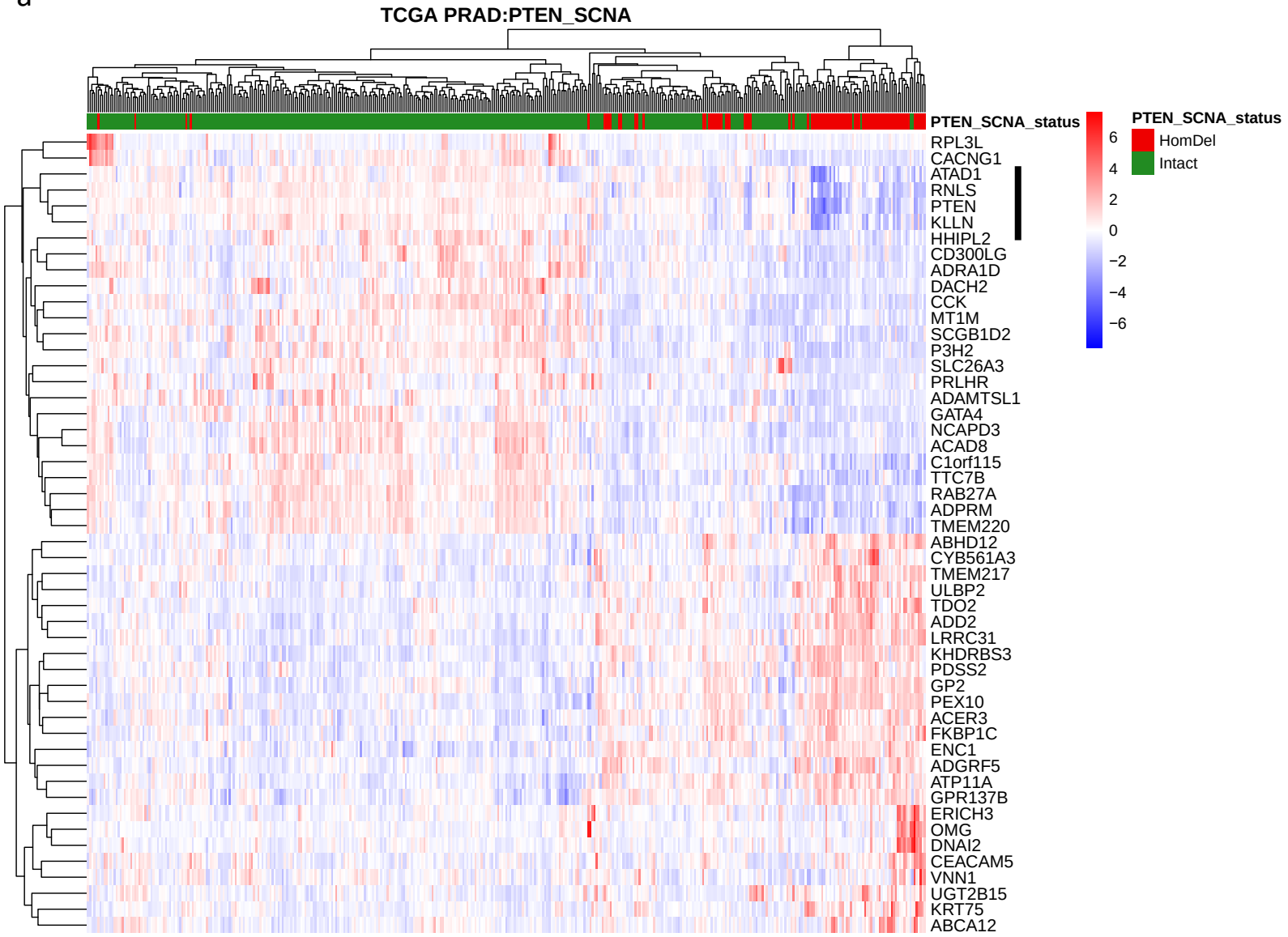

b

ID	Description	qvalue
GO:0044770	cell cycle phase transition	1,09E+12
GO:0007059	chromosome segregation	1,39E+12
GO:0007018	microtubule-based movement	2,92E+11
GO:1901987	regulation of cell cycle phase transition	4,63E+12
GO:0006281	DNA repair	6,03E+11
GO:0000819	sister chromatid segregation	0.0017
GO:0000070	mitotic sister chromatid segregation	0.0017
GO:0044782	cilium organization	0.0017
GO:0001578	microtubule bundle formation	0.0020
GO:0048285	organelle fission	0.0033

c

ID	Description	qvalue
GO:0008015	blood circulation	8,75E+09
GO:0006936	muscle contraction	1,16E+11
GO:0003018	vascular process in circulatory system	3,47E+11
GO:0034765	regulation of ion transmembrane transport	4,05E+11
GO:0099177	regulation of trans-synaptic signaling	0.0011
GO:0015844	monoamine transport	0.0022
GO:0008016	regulation of heart contraction	0.0038
GO:0016054	organic acid catabolic process	0.0041
GO:0072503	cellular divalent inorganic cation homeostasis	0.0041
GO:0007188	adenylate cyclase-modulating G protein-coupled receptor signaling pathway	0.0041

Supplementary figure 6

a

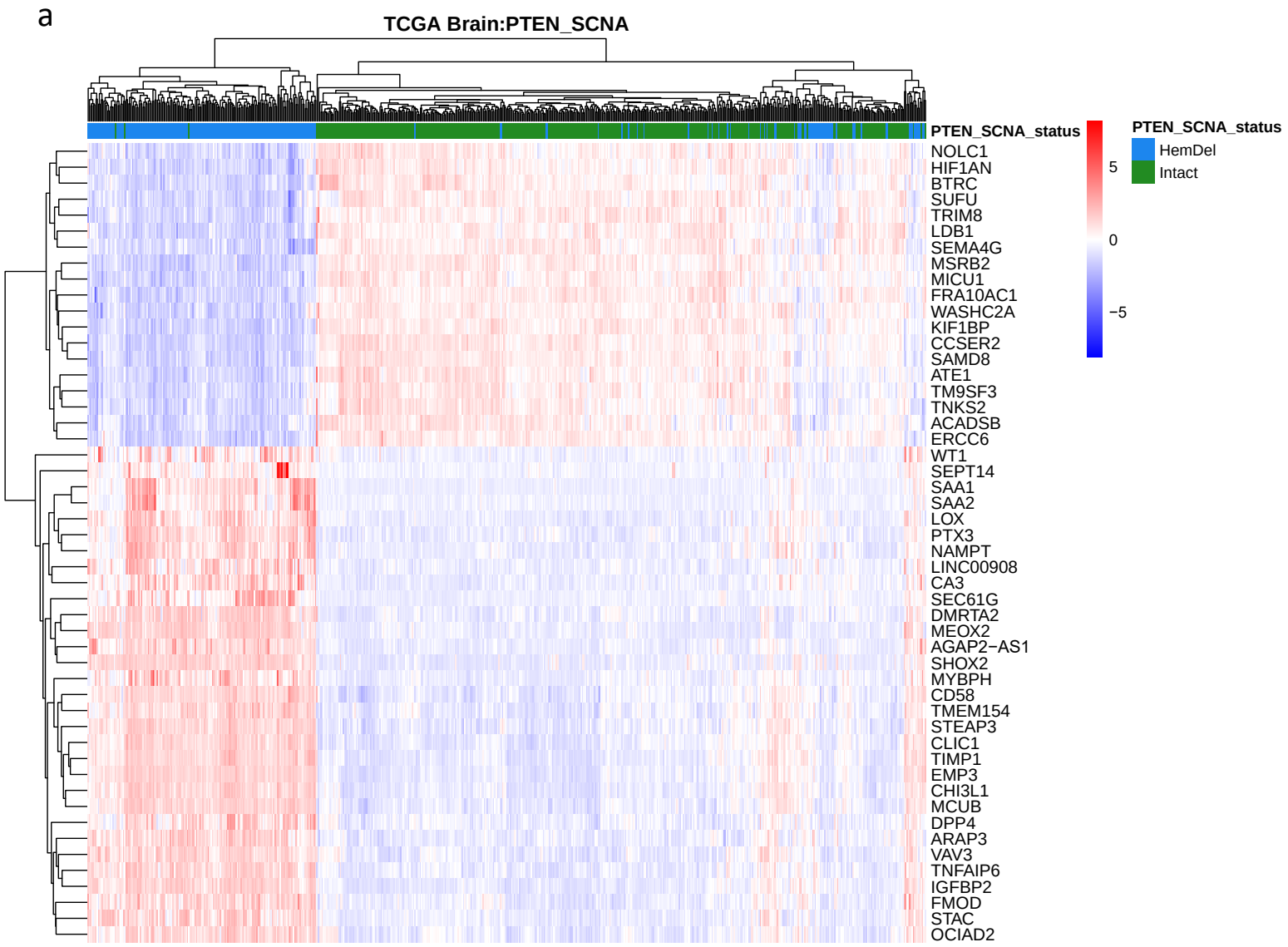

b

ID	Description	qvalue
GO:0002250	adaptive immune response	9,17E-10
GO:0042110	T cell activation	3,96E-06
GO:0030198	extracellular matrix organization	5,64E-05
GO:0002443	leukocyte mediated immunity	2,69E-01
GO:0002237	response to molecule of bacterial origin	4,85E-01
GO:0045785	positive regulation of cell adhesion	6,54E-02
GO:1903037	regulation of leukocyte cell-cell adhesion	7,12E-02
GO:0007159	leukocyte cell-cell adhesion	1,31E+00
GO:0050900	leukocyte migration	1,39E-01
GO:0050863	regulation of T cell activation	2,64E+00

c

ID	Description	qvalue
GO:0022613	ribonucleoprotein complex biogenesis	1,67E+08
GO:0008380	RNA splicing	1,67E+08
GO:0050804	modulation of chemical synaptic transmission	2,70E+10
GO:0099003	vesicle-mediated transport in synapse	6,22E+09
GO:0022618	ribonucleoprotein complex assembly	8,34E+09
GO:0071826	ribonucleoprotein complex subunit organization	1,97E+11
GO:0050808	synapse organization	5,09E+10
GO:0016197	endosomal transport	5,10E+11
GO:0043543	protein acylation	7,89E+10
GO:0001505	regulation of neurotransmitter levels	8,50E+11

Supplementary figure 7

a

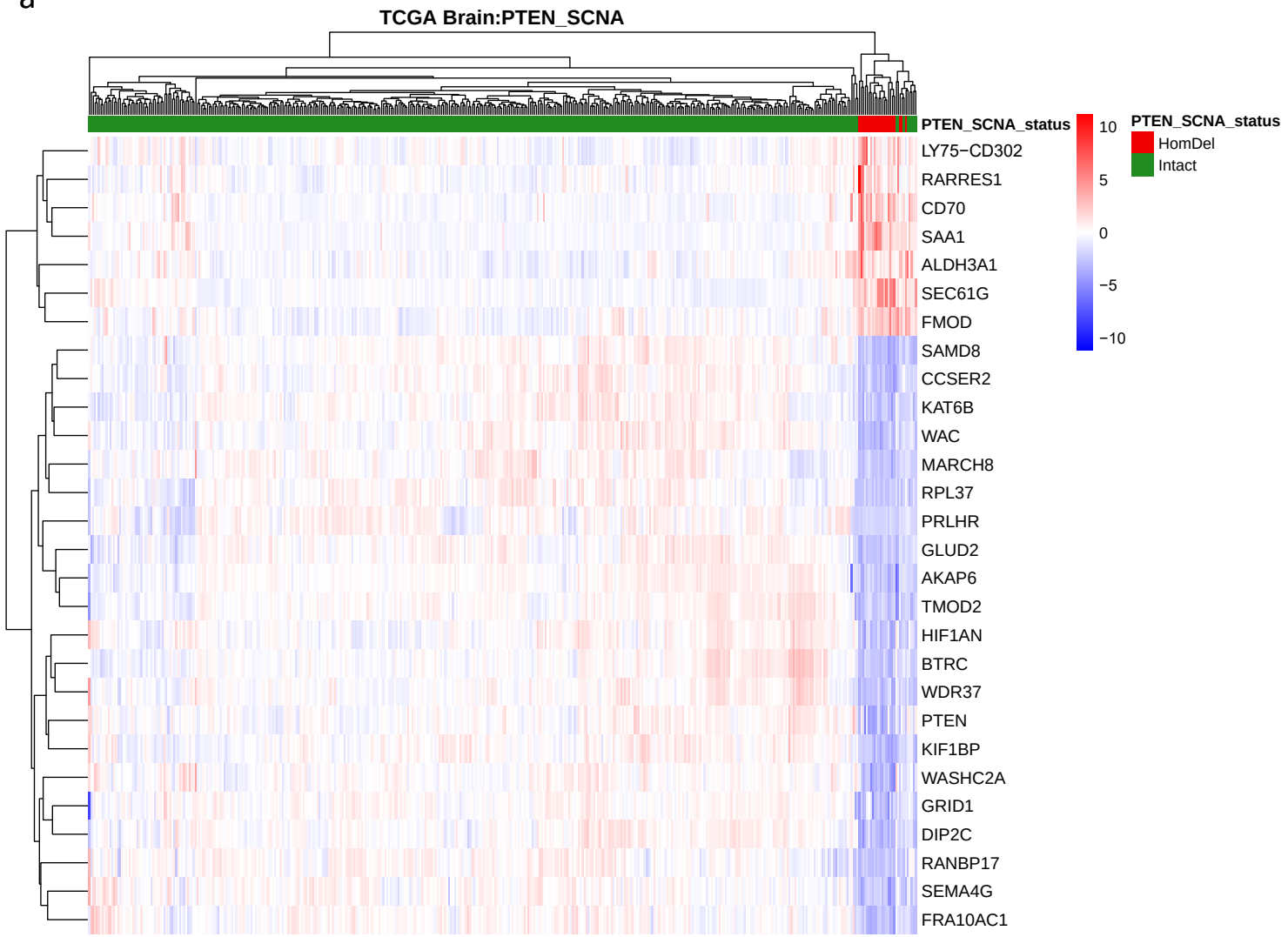

b

ID	Description	qvalue
GO:0002250	adaptive immune response	4,71E-13
GO:0042110	T cell activation	2,76E-09
GO:0050867	positive regulation of cell activation	3,49E-08
GO:0002443	leukocyte mediated immunity	7,82E-08
GO:1903037	regulation of leukocyte cell-cell adhesion	2,31E-06
GO:0050778	positive regulation of immune response	3,60E-05
GO:0007159	leukocyte cell-cell adhesion	7,56E-06
GO:0019221	cytokine-mediated signaling pathway	7,58E-06
GO:0050870	positive regulation of T cell activation	1,71E-02
GO:0001819	positive regulation of cytokine production	1,10E-01

c

ID	Description	qvalue
GO:0050804	modulation of chemical synaptic transmission	1,60E+01
GO:0099177	regulation of trans-synaptic signaling	1,60E+01
GO:0099504	synaptic vesicle cycle	2,43E+03
GO:0050808	synapse organization	9,90E+04
GO:0006397	mRNA processing	2,35E+08
GO:0016079	synaptic vesicle exocytosis	2,35E+08
GO:0060078	regulation of postsynaptic membrane potential	7,11E+07
GO:0099643	signal release from synapse	1,55E+09
GO:0016358	dendrite development	5,48E+08
GO:0001505	regulation of neurotransmitter levels	1,31E+09

Supplementary figure 8

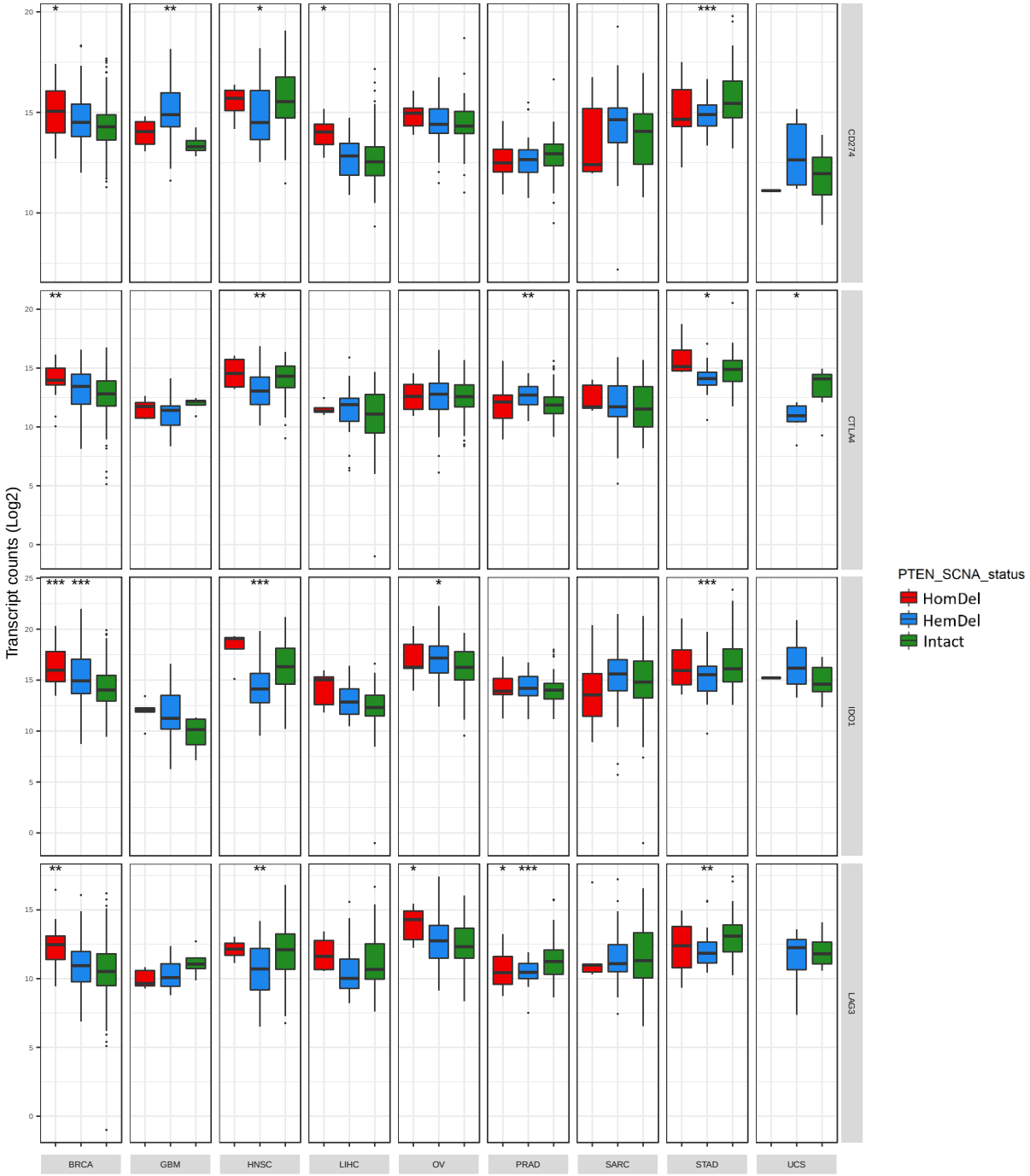

Supplementary figure 9

a

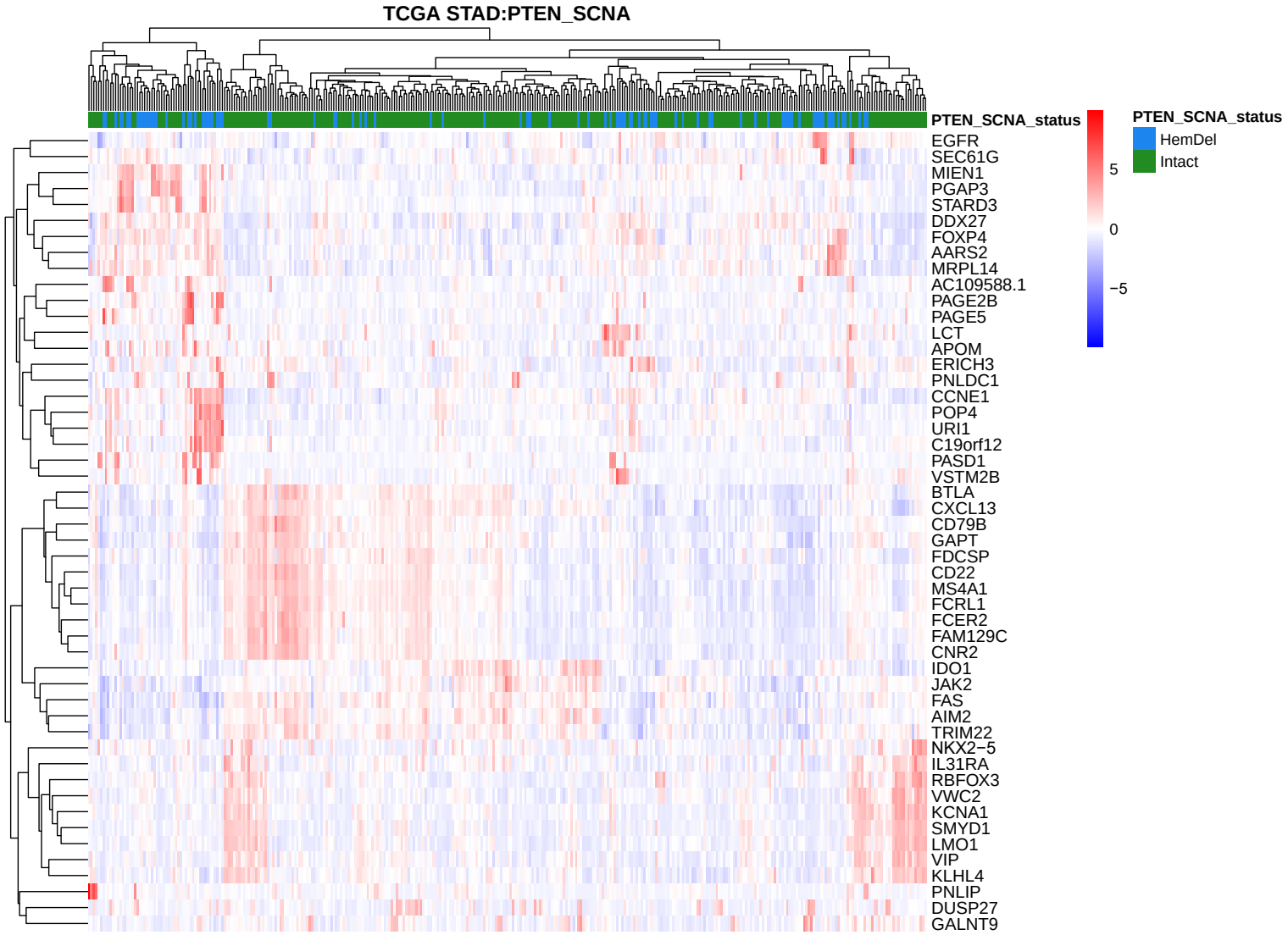

b

ID	Description	qvalue
GO:0000819	sister chromatid segregation	1,75E+06
GO:0000070	mitotic sister chromatid segregation	1,75E+06
GO:0007059	chromosome segregation	2,77E+07
GO:0000280	nuclear division	2,77E+07
GO:0098813	nuclear chromosome segregation	5,81E+06
GO:0051321	meiotic cell cycle	1,05E+12
GO:0016126	sterol biosynthetic process	5,01E+11
GO:0006695	cholesterol biosynthetic process	5,01E+11
GO:1902653	secondary alcohol biosynthetic process	5,01E+11
GO:0034660	ncRNA metabolic process	7,25E+11

c

ID	Description	qvalue
GO:0002250	adaptive immune response	1,55E-22
GO:0051249	regulation of lymphocyte activation	5,34E-12
GO:0042110	T cell activation	7,73E-12
GO:0050778	positive regulation of immune response	9,10E-11
GO:0002443	leukocyte mediated immunity	8,74E-09
GO:0007159	leukocyte cell-cell adhesion	3,17E-07
GO:1903037	regulation of leukocyte cell-cell adhesion	4,46E-07
GO:0050867	positive regulation of cell activation	7,92E-07
GO:0070661	leukocyte proliferation	4,32E-06
GO:0046651	lymphocyte proliferation	1,44E-04

Supplementary figure 10

a

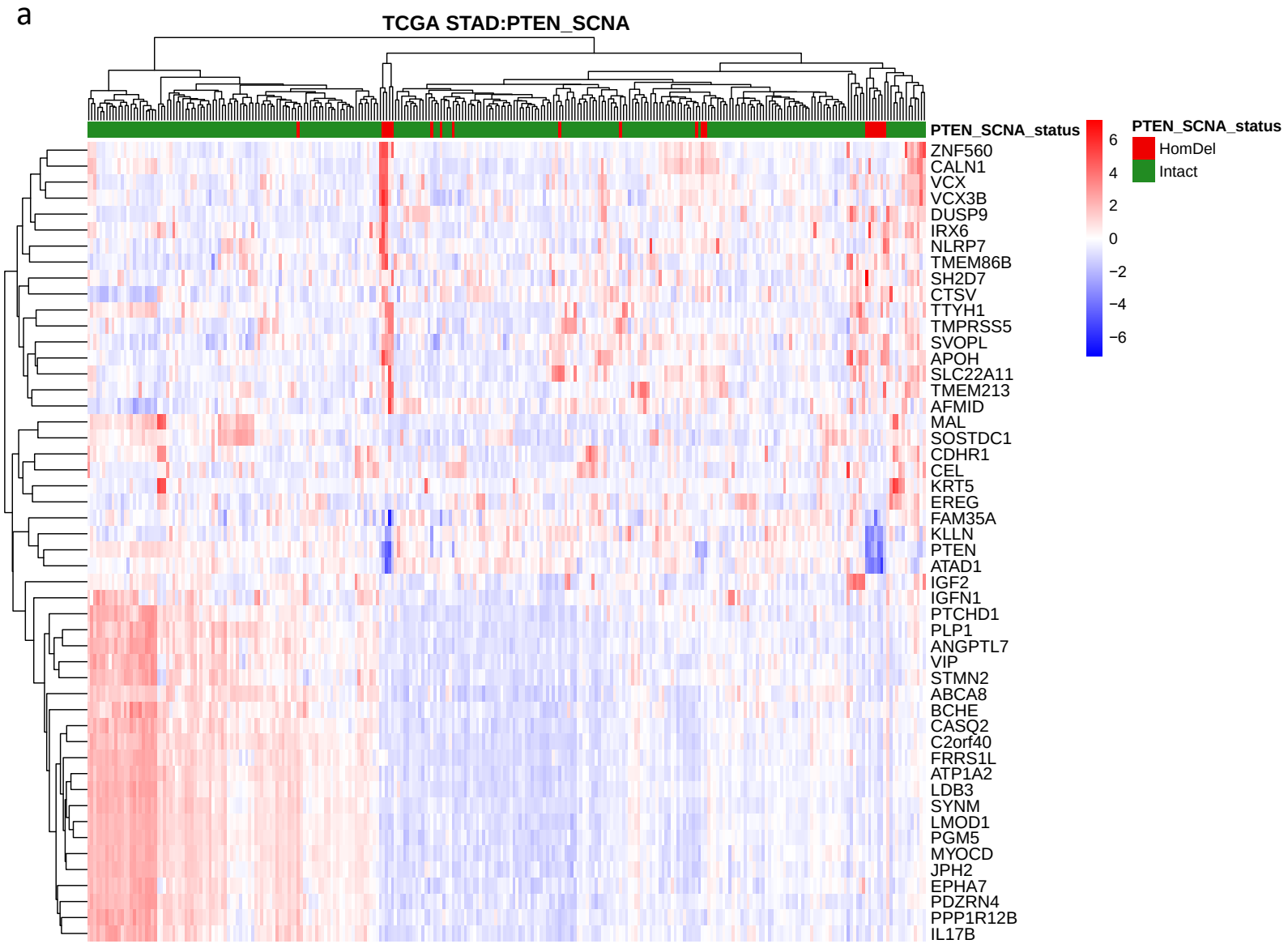

b

ID	Description	qvalue
GO:0003012	muscle system process	5,90E-07
GO:0051480	regulation of cytosolic calcium ion concentration	7,86E+02
GO:0008015	blood circulation	2,35E+04
GO:0010959	regulation of metal ion transport	7,72E+05
GO:0072507	divalent inorganic cation homeostasis	7,96E+05
GO:0008016	regulation of heart contraction	2,15E+08
GO:0042692	muscle cell differentiation	3,11E+07
GO:0060402	calcium ion transport into cytosol	5,62E+08
GO:0034765	regulation of ion transmembrane transport	7,90E+07
GO:0006816	calcium ion transport	1,21E+09

Supplementary figure 11

a

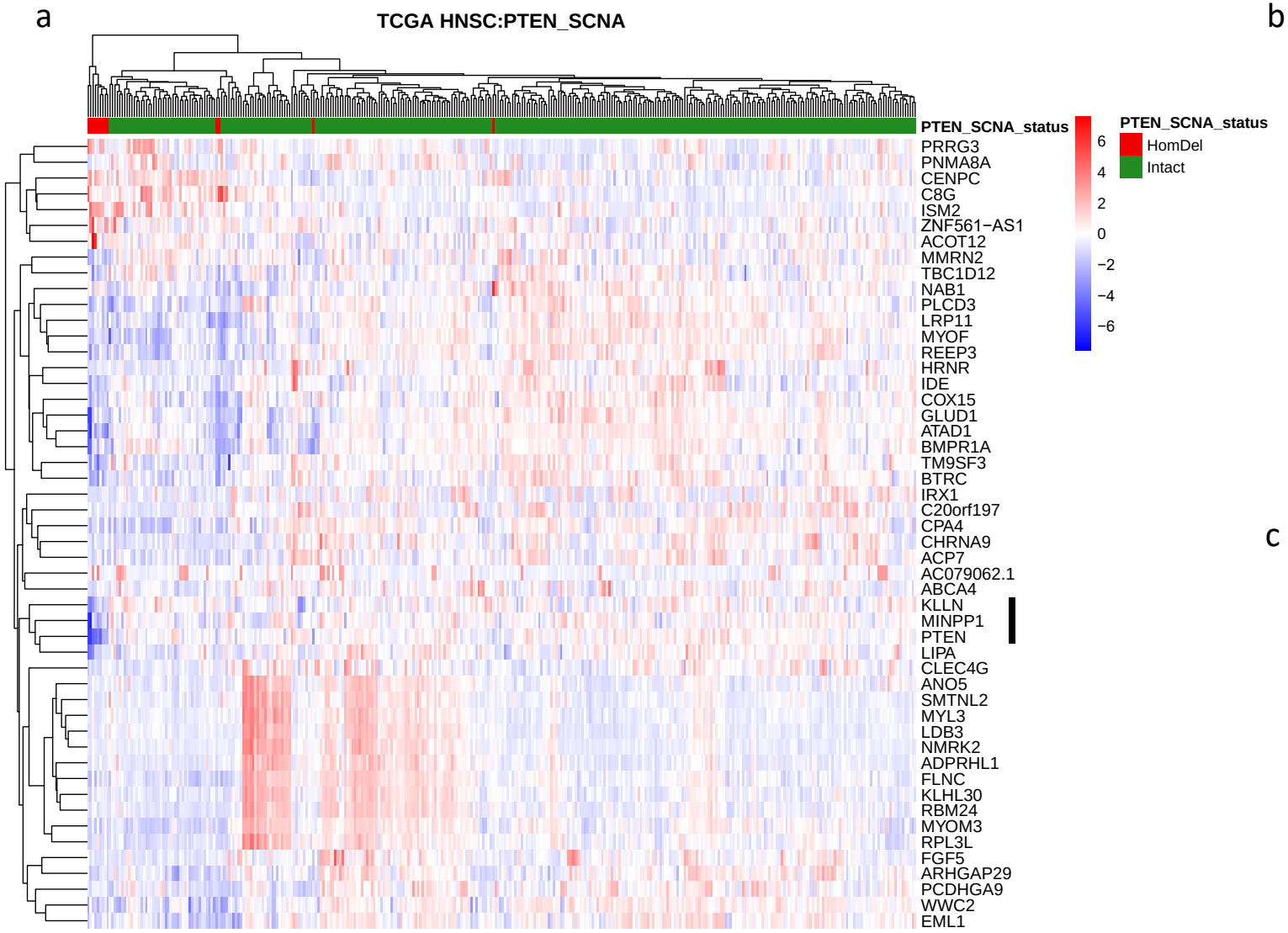

b

ID	Description	qvalue
GO:0006260	DNA replication	8,25E+09
GO:0007059	chromosome segregation	8,25E+09
GO:0051321	meiotic cell cycle	5,49E+09
GO:0098813	nuclear chromosome segregation	1,39E+12
GO:0000280	nuclear division	1,39E+12
GO:0034508	centromere complex assembly	1,92E+11
GO:0006335	DNA replication-dependent nucleosome assembly	0.0023
GO:0034723	DNA replication-dependent nucleosome organization	0.0023
GO:0071824	protein-DNA complex subunit organization	0.0028
GO:0007098	centrosome cycle	0.0028

c

ID	Description	qvalue
GO:0003012	muscle system process	2,71E-09
GO:0055001	muscle cell development	2,11E+00
GO:0014706	striated muscle tissue development	3,43E+01
GO:0030239	myofibril assembly	7,66E+00
GO:0007517	muscle organ development	2,85E+04
GO:0031032	actomyosin structure organization	3,33E+04
GO:0048738	cardiac muscle tissue development	3,80E+04
GO:0050879	multicellular organismal movement	6,46E+04
GO:0050881	musculoskeletal movement	6,46E+04
GO:0008015	blood circulation	3,51E+06

Supplementary figure 12

a

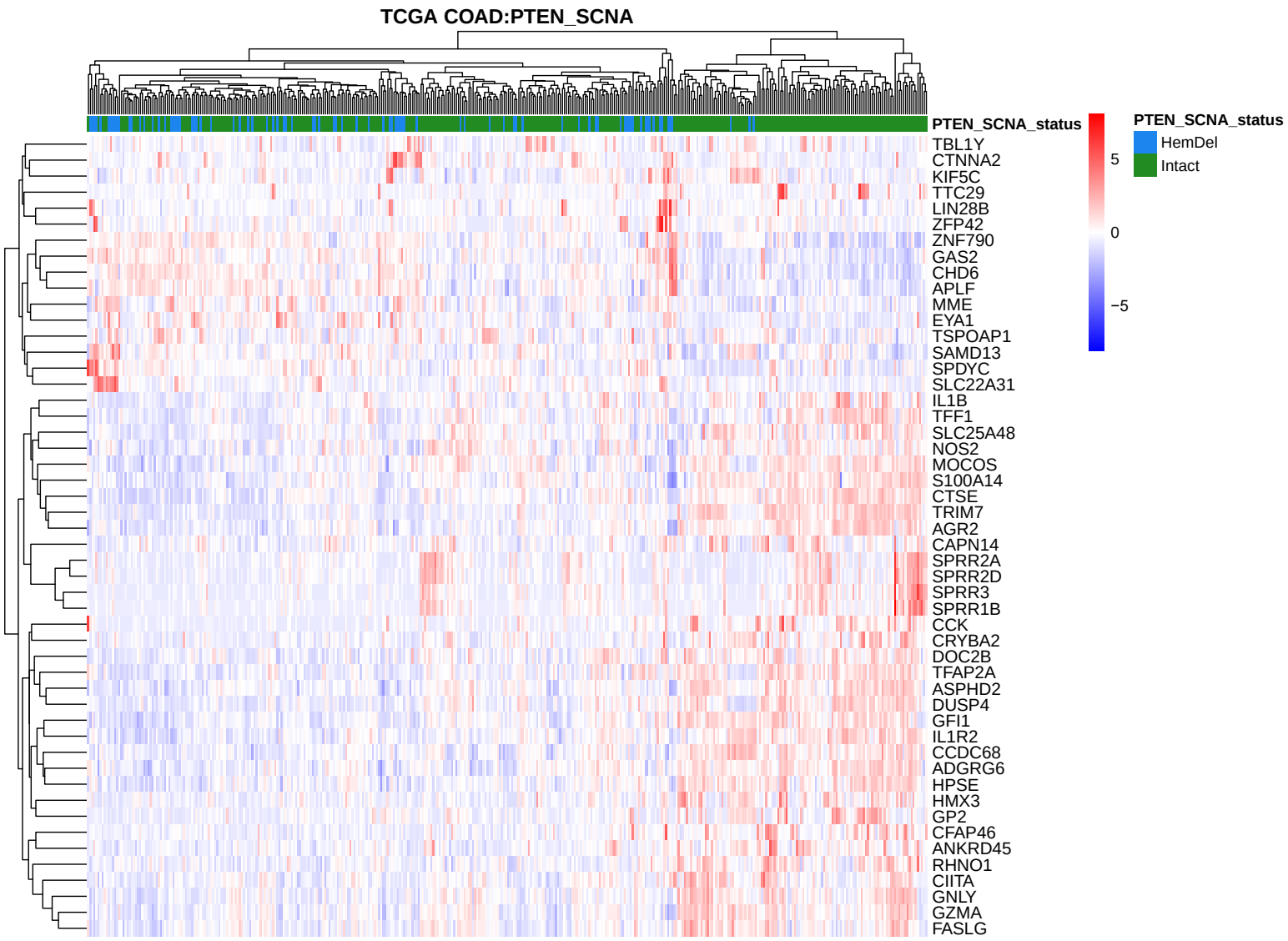

b

ID	Description	qvalue
GO:0034341	response to interferon-gamma	1,93E+10
GO:0002449	lymphocyte mediated immunity	1,93E+10
GO:0002250	adaptive immune response	1,93E+10
GO:0002228	natural killer cell mediated immunity	8,21E+10
GO:0045333	cellular respiration	1,12E+12
GO:0002396	MHC protein complex assembly	2,46E+12
GO:0001906	cell killing	2,49E+12
GO:0009615	response to virus	2,49E+12
GO:0001909	leukocyte mediated cytotoxicity	3,67E+12
GO:0002495	antigen processing and presentation of peptide antigen via MHC class II	3,67E+12

Supplementary figure 13

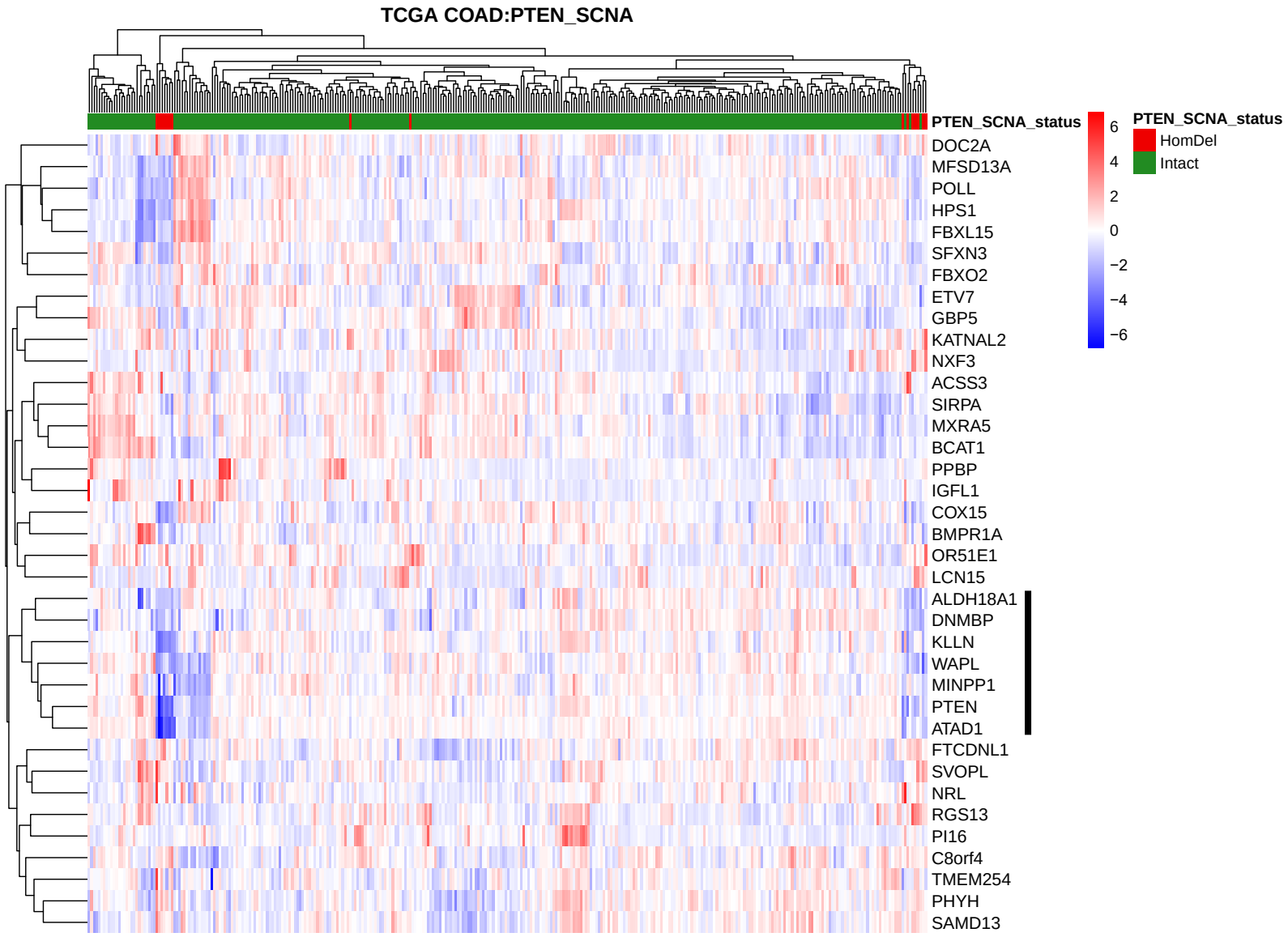

Supplementary figure 14

a

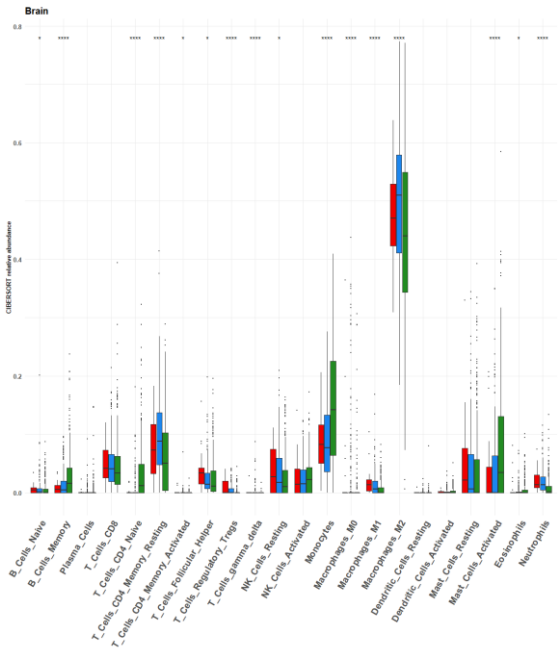

b

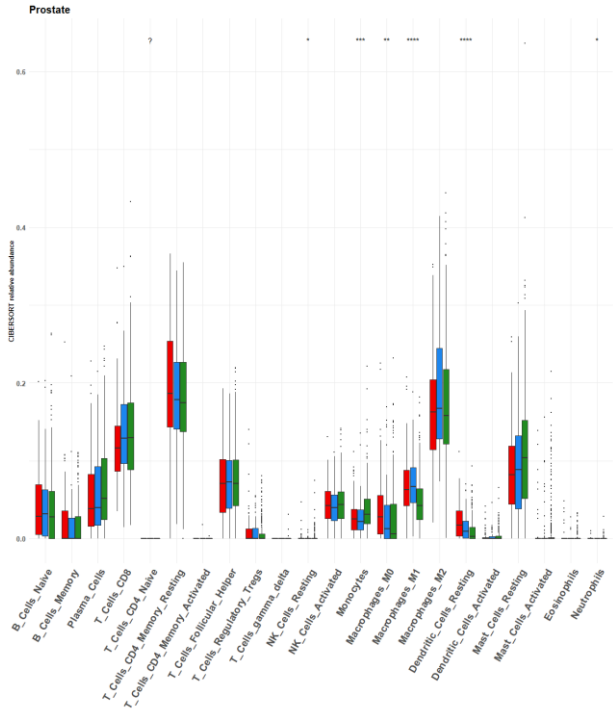

c

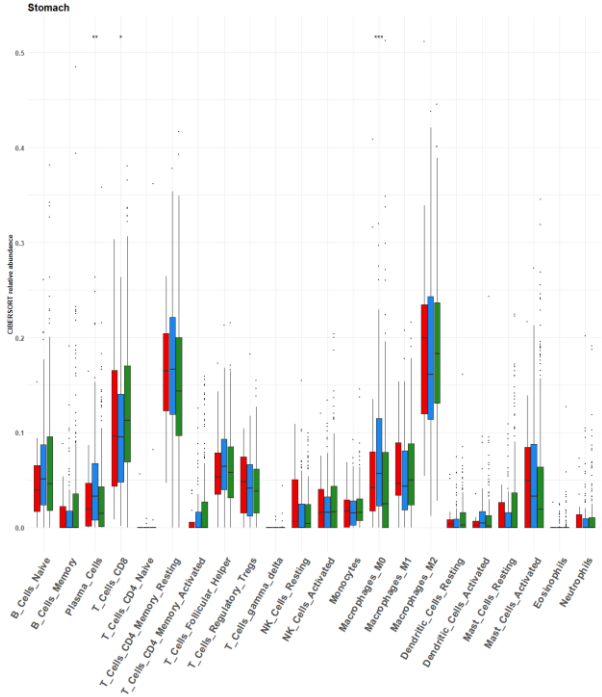

d

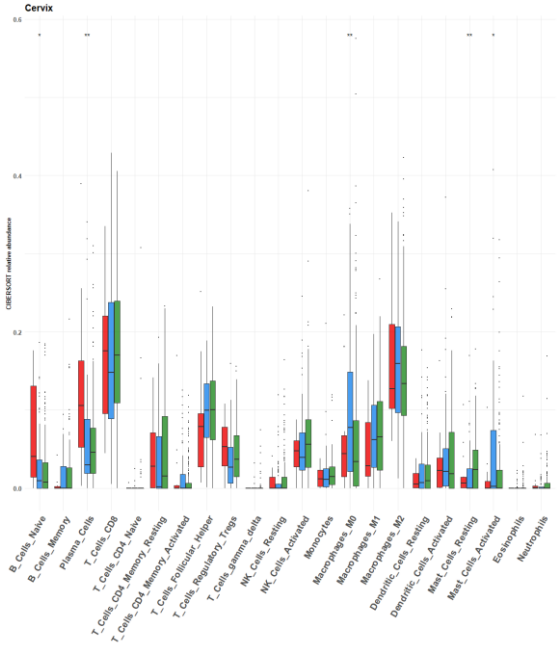

e

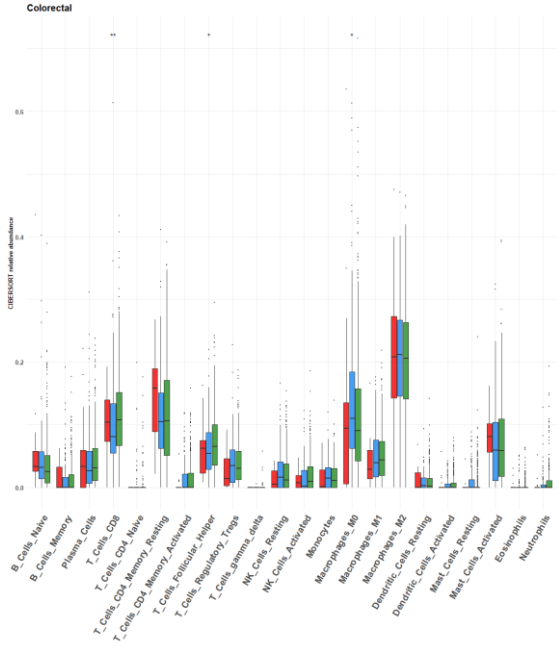

PTEN_SCNA_status
- HomDel
- HemDel
- Intact